Maria Bergemann and Camilla Juul Hansen and Timothy C. Beers[1]

[1] Max Planck Institute for Astronomy, Heidelberg
[2] University of Notre Dame

1

Phenomenology and physics of late-type stars

1.1 Introduction

Stellar astrophysics has evidenced revolutionary advances during the past decades. The advent of large-scale stellar surveys on telescopes equipped with highly-sensitive detectors has transformed our understanding of the physics of stellar atmospheres and their interiors. Detailed abundances, stellar parameters, and kinematics, which are now available for more than a million stars, are also pre-requisites for understanding the evolution of the Milky Way and its stellar populations. The main reason for the unique constraining power of stars is that they form an exceptionally diverse class of cosmic objects, with physical conditions spanning many orders of magnitude. In the Sun alone, density changes from $\rho_{\rm core} \sim 10^2$ g/cm^3 in the core to $\rho_{\rm surface} \sim 10^{-7}$ g/cm^3 in the photosphere (and five orders of magnitude less in the chromosphere), and the local kinetic temperature drops from $T_{\rm core} \sim 10^7$ K to $T_{\rm surface} \sim 6000$ K in the outer layers. For a red supergiant with a mass of 10 $M_\odot$, this change is even more dramatic, from $\rho_{\rm core} \sim 10^5$ g/cm^3 to $\sim 10^{-15}$ g/cm^3 at base of the wind above the photosphere.

The immense variation of the internal stellar conditions reflects the complex nature of phenomena occurring in their interiors and surfaces. Physical theory allows the existence of "living"[1] stars as small as only 8% of the mass and radius of our own star, the ultra-cool M dwarfs, but also stars that exceed the radius of the Solar System in size. The extreme contrast between the macro-physics, that is, the global phenomena acting on the surfaces and in interiors of stars, such as convection, pulsation, winds, and mass loss, and also the micro-physics, which is needed to model the production and transport of energy, implies an extraordinary complexity of the theoretical models required to make robust predictions of the properties of stars.

[1] Here we refrain from the so-called dead stars, stellar remnants such as white dwarfs, neutron stars, or black holes, which may have much smaller radii.

Thus, stars are indeed the ideal plasma physics laboratories, offering a window into conditions that cannot be achieved elsewhere.

In this review, we focus on the so-called "cool", late-type, stars, which represent spectral classes F,G,K, and M (Fig 1.1). The effective temperature, $T_{\rm eff}$, at the surface of these objects does not change greatly, at most by a factor of two, from a typical red supergiant ($T_{\rm eff} \sim 3400$ K) to a typical hot main-sequence turn-off star ($T_{\rm eff} \sim 6500 - 7000$ K). However, cool stars possess other remarkable characteristics, which make them the most robust and useful tracers of the evolutionary history of their parent populations. First, the unevolved stars on the main sequence preserve the natal composition of the gas cloud from which they formed. Secondly, the lifetimes of cool stars range from a few million years for the most massive stars to over a Hubble time for the least massive stars. Thirdly, cool stars span an enormous range in luminosity ($L = 4\pi R^2 \sigma_{\rm SB} T_{\rm eff}^4$), which reflects the variation in the radius R and in the total emitted flux ($F_{tot} = \sigma_{\rm SB} T_{\rm eff}^4$). Indeed, the most luminous stars, with $L \sim 10^5$ $L_\odot$ can nowadays be seen with 10-m telescopes to distances of Mpc (millions of parsecs; Evans et al. 2011). Also, ongoing large stellar surveys are discovering low-metallicity stars with ages greater than 13 Gyr (Frebel and Norris, 2015). These are the best candidates for probing the physical state of the very early Galaxy and the conditions in the early Universe, at a level of detail superior to any study of ultra-high-redshift galaxies.

The physics of cool stars is extremely complex, therefore in this chapter we are not aiming to provide a comprehensive overview of all the major developments that have occurred over the past decade. Neither is this meant to be an in-depth study of any particular subject. The main goal of this article is to set the scene, and to give the flavour of the current research in modelling and observations of late-type stars, with a focus on their atmospheres. We will also mention the applications of these data in studies of other astronomical domains. Models of stellar spectra are used in most fields in contemporary astrophysics, from studies of stellar evolution to exo-planet spectra, populations synthesis, and galaxy formation. Observations of stellar abundances even have implications for cosmology. Therefore, it seems very timely to review the present state of these studies, and draw an outlook for future studies.

This chapter is structured as follows. We summarise the main observational constraints on the physical properties of cool stars and outline briefly their evolution in Section 1.2. Model atmosphere and synthetic spectra, which are needed for the quantitative diagnostic of the observations, are reviewed in Section 1.3. Section 1.4 presents a brief recap on stellar nucleosynthesis. Section 1.5 introduces the reader to the fields of stellar populations and Galactic chemical evolution, and mentions some outstanding science cases, which have been resolved and/or triggered by new

observations or by application of the new models. We close with some conclusions and an outlook for the future in Section 1.6.

1.2 Observations of cool stars

1.2.1 Terminology

Astronomers love acronyms, and below the reader will encounter many. In this section a short overview of various types of stars and terminology will be given. The fundamental parameters of stars, which set their evolutionary paths, are their mass and chemical composition. However, from an observer's perspective, it is common to characterise stars by their effective temperature, surface gravity, and metallicity. The latter classification is also approximate, as it stems from the historical effort to employ one-dimensional hydrostatic plane-parallel model atmospheres, which are semi-infinite (and thus have no size); the gravitational acceleration at the surface, log (g), as well as the bolometric flux, are assumed to be constant as well. Throughout the discussion in the next sections, it should be kept in mind that these are just a set of approximations, and the standard quantities, $T_{\rm eff}$, log(g), and [Fe/H], are not the fundamental parameters of stars, per se.

Metallicity[2] is usually denoted as [Fe/H], i.e., the logarithmic ratio of the number of absorbing atoms of iron to hydrogen per unit volume in the star scaled to the solar ratio. The abundances are defined in the following way:

$$\log(A_{\rm Fe}) = \log(N_{\rm Fe}/N_{\rm H}) + 12 \quad (1.1)$$

$$[{\rm Fe/H}] = \log(A_{\rm Fe,star}) - \log(A_{\rm Fe,\odot}) \quad (1.2)$$

$$[{\rm Mg/Fe}] = [{\rm Mg/H}] - [{\rm Fe/H}] = \log({\rm A_{Mg,star}}) - \log({\rm A_{Mg,\odot}}) - [{\rm Fe/H}] \quad (1.3)$$

In this notation, the Sun has [Fe/H] = 0 and *zero* abundance of any other element relative to metallicity, i.e., for example [Mg/Fe] = 0. Based on this value, the star will either be sub-solar ([Fe/H] < 0) or super-solar ([Fe/H] > 0). It is sometimes convenient to have a finer division of the sub-solar metallicities, because chemical traces of many nuclear processes are most easily found at various levels below solar metallicity (see Table 1.1), and in some specialised research fields, only individual metallicity bins are important. These notations are not binding, and it is common in astronomical literature to refer to all cool stars with [Fe/H] < −1 simply as metal-poor stars.

The effect of metallicity on the blue regions of stellar spectra is shown in Fig. 1.1.

[2] In astronomy, every element beyond He is referred to as a 'metal'.

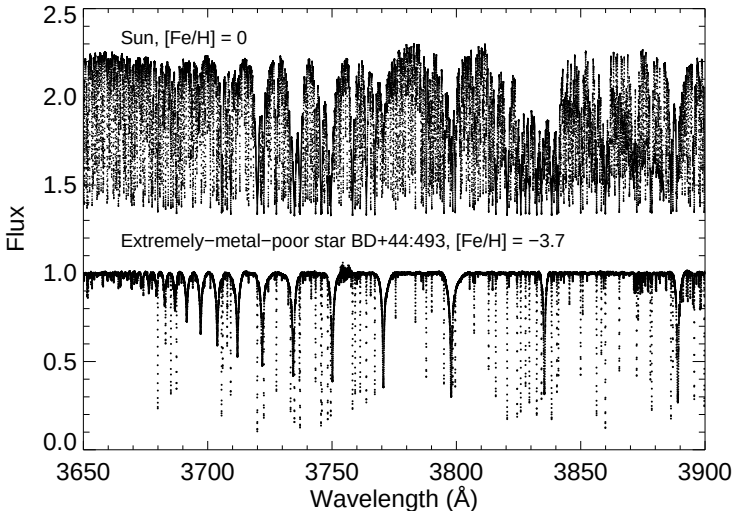

Figure 1.1 Blue regions of high-resolution spectra observed for the Sun (KPNO) and the HDS/Subaru spectrum of a carbon-enhanced metal-poor (CEMP) star, BD+44^{o}493 (Ito et al., 2013). Note the dramatic contrast in the number of spectral lines seen in these stars, which differ in metallicity by about four orders of magnitude.

This wavelength regime is most sensitive to the metallicity of a star, because it hosts the largest number of metallic lines.

The classification based on mass is derived from stellar evolution theory, and represents qualitatively different paths taken by stars in a given mass range. Stars less than 2 $M_\odot$ are usually referred to as low-mass stars. Stars with mass from 2 to $\sim 7/10$ $M_\odot$ are intermediate-mass objects, and those with even higher masses are "massive" stars. The evolutionary paths of these objects are described briefly in the next section.

Table 1.1 *A common classification of cool stars by metallicity (Beers and Christlieb, 2005).*

Term	Acronym	[Fe/H]
Metal-rich	MR	[Fe/H] > 0
Metal-poor	MP	[Fe/H] < -1
Very metal-poor	VMP	[Fe/H] < -2
Extremely metal-poor	EMP	[Fe/H] < -3
Ultra metal-poor	UMP	[Fe/H] < -4
Hyper metal-poor	HMP	[Fe/H] < -5
Mega metal-poor	MMP	[Fe/H] < -6

1.2.2 A brief sketch of the evolution of low- and intermediate-mass stars

Stars live through one of two ways – contraction or nuclear burning. For the star to end up on the main sequence, where nuclear burning in the core sets in, the star must first undergo a phase of contraction[3] to achieve a temperature in the core sufficient to initiate nuclear reactions. Stellar evolution then proceeds as follows. Nuclei with the lowest Coulomb barrier, starting with hydrogen, burn first, until the fuel is exhausted in the core and the core contracts, increasing its temperature, until the conditions allow ignition of nuclei with the next lowest Coulomb barrier, and so forth. Fusion may also occur in the layers outside the core, forming the famous "onion-shell" structure in massive stars. In this way, the chemical composition inside the star changes. Internal mixing processes during later evolutionary stages can bring a portion of this material to the surface, which is the region we can observe and derive abundances for.

Figure 1.2 shows a typical diagram representing the evolution of cool stars. The

[3] The Kelvin-Helmholtz contraction, caused by cooling at the surface of a star and pressure drop, leads to compression and heating in the core.

definition of a cool star is very broad, and includes both low- and high-mass stars in different evolutionary stages, or even in different systems, for example, single stars and binaries. In particular, we find main-sequence stars, sub-giants, red giants, and asymptotic giant branch stars, which are simply different stages of evolution for low-mass stars.

- Main sequence (MS)
  Inspecting figure 1.2 more closely, we find that the lower part of the diagram is occupied by stars on the MS, those which fuse hydrogen into helium in the core. Stars spend the majority of their lifetimes on the MS. For a typical 1 M_{Sun} star like the Sun, the MS lifetime is $\sim$ 9 Gyr. Once the core H reservoir is depleted, the star starts contracting, and as the outer layers heat up, H burning is ignited in a shell. This is when the star turns off the main sequence. Turnoff stars are extremely important for studies of stellar populations, because their ages can be accurately determined through isochrone fitting (Soderblom, 2010).
- Turn-off (TO) and sub-giant (SG)
  After the TO, the star becomes more luminous, but cooler, and moves onto the sub-giant branch, where it undergoes hydrogen shell burning. The SG branch, although representing a short evolutionary stage, is also important as an age diagnostic for individual stars, because this is the locus where the tracks of different ages and metallicities do not overlap. The mass of the He core grows through the ashes of H burning in the shell, and, at a certain point, the core becomes degenerate[4]. This is when the star moves onto the red giant branch. Due to the expansion and the surface cooling of a star, the envelope becomes convective, allowing more efficient outward energy transport.
- Red Giant Branch (RGB)
  Subsequent H burning in the shell goes on via the CNO cycle. The star moves almost vertically in the $T_{\rm eff}$-log(g) diagram, maintaining its total flux, but rapidly increasing the luminosity and radius. RGB stars are more luminous and cooler than the MS stars, typically with $T_{\rm eff} < 5200$ K and surface gravities of log(g) $<$ 3, yet luminosities up to $10^3\ L_\odot$. The first dredge-up takes place on the ascending part of the RGB, when the products of H burning are mixed up to the surface through large-scale convection. The surface is then enriched in ^{13}C and in N, but depleted in Be, Li, and ^{12}C.

  The tip of the RGB is determined by the luminosity at which stars experience the He flash, in which He ignition occurs as a runaway process, due to electron degeneracy decoupling pressure from temperature. When enough thermal energy has been released, degeneracy is lifted, and the runaway process halts. All stars at the tip of the RGB possess He cores of $\approx$ 0.5 $M_\odot$, and similar luminosi-

[4] This only happens for lower-mass stars.

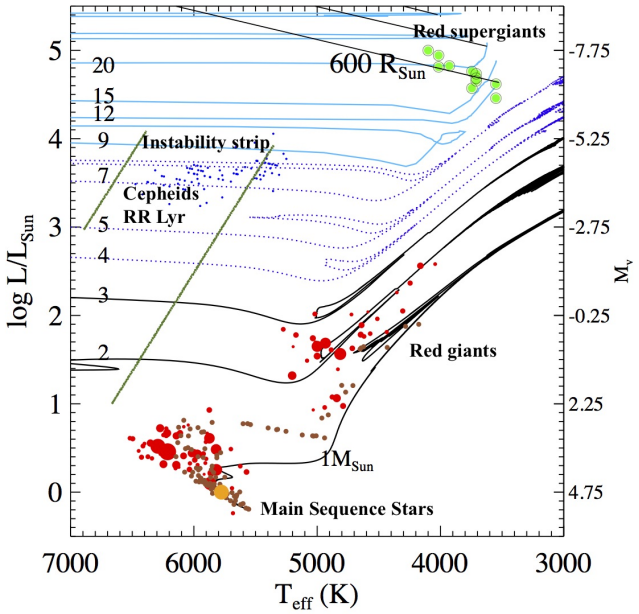

Figure 1.2 The evolutionary $T_{\rm eff}$ - luminosity diagram for cool stars. The blue dots represent the observed data for Cepheids in the Milky Way (Genovali et al., 2014). Other observed datasets were taken from Ruchti et al. (2013), Gazak et al. (2014), and Pace et al. (2012).

ties, which makes them a powerful diagnostic of extragalactic distances, as they are "standard candles" (Salaris, 2012). The most recent studies indicate that the impact of physics on stellar evolutionary models is significant, and may have an effect on the determination of the Hubble constant, H_0, using the tip of the RGB method, on the order of few percent (Serenelli et al., 2017).

- Horizontal branch (HB)
  After the tip of the RGB stage, the star moves into a new equilibrium configuration, in which He burning occurs in the core under non-degenerate conditions, with H burning in a shell. This phase lasts about 10^8 years, and the star radiates with a luminosity of $\sim$ 50-100 $L_{\odot}$. HB stars are easier to detect in globular clusters (GCs) than in the field, and they offer an independent way of determining the age of a GC, because the HB morphology depends on both age and metallicity (Catelan, 2009). The coolest end of the HB is also termed the "red clump" (RC). The stars of solar-like metallicity pile up there, because the masses of He degenerate cores are nearly equal. However, the mass of the H-burning envelope also matters for the location of a core He-burning star in the $T_{\rm eff}$-log(g) plane,

and this depends on the metallicity. In metal-poor GCs, the HB is extended to higher temperatures (or bluer colours), due to the presence of old low-metallicity stars with thin H envelopes.

It is barely possible to spectroscopically distinguish between ascending and descending (towards the RC and core He-burning phase) stage, although attempts have been made recently using indirect methods coupled to the data from asteroseismology (Ness et al., 2016).

- Asymptotic giant branch (AGB)
  After exhaustion of He in the core, the star consists of a C/O-core, a shell that burns He to C, an inter-shell consisting of He, followed by a thin shell where H burns to He. The outer H-rich envelope is convective. During this phase, the star experiences multiple He shell flashes. Slow neutron-capture (*s*-process) nucleosynthesis occurs in ^{13}C-rich pockets, and the products are mixed up to the surface during the thermal pulses (Karakas and Lattanzio, 2014).

The final stages of stellar evolution will depend critically on the initial mass and metallicity of a star, but also on the mass loss. These stages are summarised in Table 1.2 .

Other members of the cool star group include objects on the instability strip (RR Lyrae, Cepheids), as well as red supergiants (RSGs), which are massive OB stars that have evolved from the main-sequence. RSGs have enormous radii, up to 1500 $R_{\odot}$, but temperatures rarely greater than $\sim$ 4300 K (Davies et al., 2013). The atmospheres of RSGs are extremely diffuse, with gravitational acceleration at the surface of $\log(g) \lesssim 1$.

It is common to distinguish pulsating stars, those on the instability strip, from non-pulsating stars. However, this picture is not physically correct. Indeed, all stars oscillate, although oscillation periods (minutes to years), amplitudes (parts per million, ppm), and the physical mechanisms driving pulsations are different (Gautschy and Saio, 1995). Oscillations of the Sun are stochastically excited by mass motions in the outer convective zone, and are particularly strong at frequencies around 3 mHz, – the so-called 5-minute oscillations. This is also the mechanism that drives low-amplitude oscillations of MS and RGB stars (solar-like oscillations; Chaplin and Miglio 2013).

Cepheids and RR Lyrae are the most prominent members of the radially pulsating group, which change their radii by up to 20% during pulsations. Cepheids occur in two types: Type I, young intermediate-to-massive stars with 5-10 $M_{\odot}$, and Type II, old metal-poor stars with very low mass (M$\sim$ 0.5 $M_{\rm Sun}$). Type I Cepheids have short periods, from less than a day to a few weeks, whereas Type II Cepheids pulsate with longer periods, of a few to $\sim$ 50 days (Bono et al., 1997; Wallerstein, 2002). Cepheids are classical fundamental mode pulsators, which experience self-

Table 1.2 *Evolutionary paths of stars with different ZAMS masses (courtesy A. Serenelli).*

Class	Mass range ($M_\odot$) approximate	Main nuclear energy source Evolutionary endpoint
Brown dwarfs	0.01 – 0.08	deuterium burning lithium burning (massive ones) H-degenerate cores (> Hubble time)
Very low mass stars	0.08 – 0.45	hydrogen burning helium core white dwarfs (> Hubble time)
Low mass stars	0.45 – 2	hydrogen burning helium burning (degenerate ignition) carbon/oxygen white dwarfs
Intermediate mass stars	2 – 7/10	hydrogen burning helium burning (non-degenerate ignition) carbon/oxygen white dwarfs
Massive stars	7/8 – 10/12	H-burning, He-burning carbon burning (degenerate ignition) oxygen/neon white dwarfs e- capture supernovae (neutron stars)
Very massive stars	> 10/12	H-burning, He-burning, C-burning Ne-burning, O-burning, Si-burning −− > Fe-cores Core collapse supernovae (neutron stars, black holes) no remnant for pair-instability SNe (?)

excitation, driven mostly by the κ effect, the increase in opacity with heating and compression under certain conditions. These conditions are met in the regions of partial ionisation of He or H. Physically, Type II cepheids are thought to be objects that experience shell flashes, either on the evolution towards the AGB or on the AGB, and are temporarily moved into the instability strip. Cepheids are very important as extragalactic distance indicators, and can be used to calibrate SN Ia for the determination of the Hubble constant (Madore and Freedman, 1998; Riess et al., 2011; Zhang et al., 2017).

RR Lyrae are another class of pulsating (or variable) stars. If the H envelope mass is low, the star ends up on the blue end of the horizontal branch, and is dynamically unstable, which results in cyclic pulsation. These stars have short pulsation periods, typically between 0.5 and 0.8 days (Catelan, 2009). RR Lyrae are low-mass stars, which means that they are long-lived, and the ones found in the Milky

Way today are typically $\sim 10 - 12$ Gyr old. These stars are bright, identifiable via their distinctive light-curves, and can be used to probe the earliest epochs of the formation of the Galaxy, in particular its halo and the bulge (Lee, 1992; Hansen et al., 2011; Soszyński et al., 2014; Marconi and Minniti, 2018).

Many stars occur in multiple systems, which affects not only the evolutionary path of the system, but also their surface composition. One prominent example are the Blue Stragglers (BS), which are thought to form through two channels, referred to as "collisional BS" or "mass-transfer BS". The latter refers to mass transfer from the primary massive star, which has experienced Roche lobe overflow onto the less-massive secondary. This hypothesis is supported by observations of BS in GCs, and in particular, depletion of C and O in their atmospheres (Ferraro et al., 2006).

1.2.3 Multi-messenger diagnostics

Modern instruments offer a great variety of tools that can be used to perform multi-wavelength observations of stars. Photometric observations, i.e., observations of the integrated light in a given bandpass, are most useful to globally map stellar populations or to perform deep imaging in smaller parts of the sky, centred on smaller objects (globular or open star clusters). Observations in different photometric bands offer potential diagnostics of the stellar atmosphere. The bluer bands are, in particular, quite important as $T_{\rm eff}$ and metallicity indicators. Filters in the near-UV that cover the Balmer jump can also be used as an indicator of the surface gravity (Casagrande et al., 2011). Infra-red photometry is a particularly powerful means to probe the high-extinction regions of the Milky Way, such as the disc and the bulge. Imaging from space facilities, like HST or Gaia, offer much cleaner information, devoid of the blurring and absorption/emission signatures of the Earth's atmosphere. This is particularly useful for studies of the content of distant compact stellar populations, such as globular clusters, where high angular resolution is essential.

Spectroscopy is a very powerful method to explore the surface properties of stars. Modern instruments, such as the optical spectrographs UVES at VLT, HIRES at Keck, HDS at SUBARU, or MIKE at Magellan, provide high resolving power, $R > 30\,000$, with full wavelength coverage across the optical region of several thousand angstroms from blue to red. For a bright star with magnitude $V < 12$, one may reach very high signal-to-noise ratios, thus resolving the weakest spectral lines, representing low-abundance exotic elements such as silver (Hansen et al., 2012). Spectroscopic information typically derives from a number of diagnostic features, which can be combined, e.g., by exploiting the requirement of excitation – ionisation balance to constrain the total flux ($T_{\rm eff}$) or pressure (gravitational acceleration at the surface) (Bergemann et al., 2012; Ruchti et al., 2013). Metallicity,

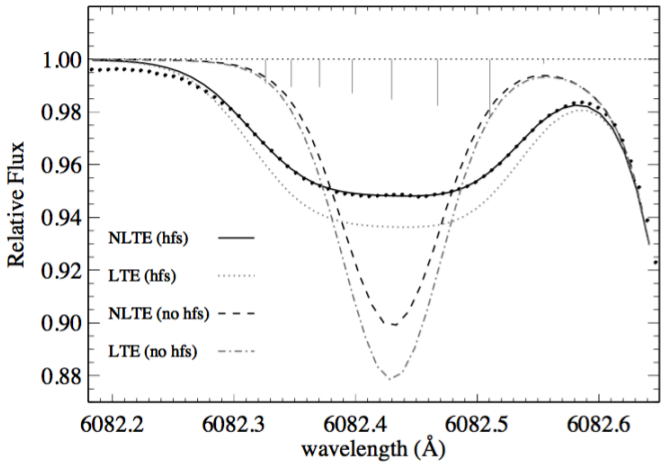

Figure 1.3 A line of neutral cobalt in the solar spectrum, computed using LTE and NLTE, with and without HFS, respectively.

or iron abundance, can be derived through the analysis of numerous iron lines. In a typical high-resolution optical spectrum of a late-type star, there are $>$ 1 million detectable lines of Fe I. The abundances of other elements can be derived from individual spectral lines, which are found all over, from the near-UV to the near-IR.

While the positions of spectral lines appear to be completely random, they are of course not, as the wavelength (or energy) simply reflects the arrangement of the energy levels in the electronic configuration system of a given atom. This, in term, depends on the atomic properties, such as the mass of the nucleus, its magnetic moment, and the number and degree of filling of the electronic shells. Some elements with non-zero magnetic moments, particularly those with odd numbers of neutrons and odd numbers of protons in the nucleus, experience splitting of energy levels due to the interaction of nuclear magnetic moments with magnetic fields produced by the outer electrons. The larger the magnetic moment, such as $5/2$ for Mn and $7/2$ for Co, the more prominent is the hyperfine splitting (HFS) of spectral lines, which is clearly distinguishable in a high-resolution stellar spectrum (Bergemann and Gehren, 2008; Bergemann et al., 2010). For some Co I lines, for example, the splitting exceeds 0.5 Å, far larger than the typical Doppler broadening caused by the thermal motions of atoms in the stellar atmosphere (Fig. 1.3). Furthermore, most elements are represented by a number of stable and un-stable isotopes in different abundance proportions. Barium is one of the species that is strongly affected by isotopic splitting, in addition to HFS.

The shapes and positions of spectral lines also convey an enormous amount of

information about the stellar surface: From the overall wavelength shift of the lines one may measure the radial velocity of the star, from the line shape the stellar rotation velocity, and, with sufficiently high-resolution spectra, the direction and velocity of mass flows at the surface (Dravins, 1999; Allende Prieto et al., 2002; Ramírez et al., 2008). At very high spatial and temporal resolution, like that available from observations of the Sun (Asplund et al., 2009; Lind et al., 2017), one may even determine the properties of convective motions from the blue- and red-shifts of individual spectral lines, which react sensitively to the atmospheric dynamics. Some spectral lines, like the Mn I 5395 Å (Danilovic et al., 2016), Ni I 6767.8 Å, and H_α 6562.8 Å lines, are also sensitive to magnetic field and velocities in stellar chromospheres (Leenaarts et al., 2012).

Stellar spectra are generally a remarkable source of information. However, not all required information can be derived from a spectrum. In particular, among the most important determinations is the evolutionary state of stars, which constrain the mass, the age, or even the position of a star on the RGB. Recent purely empirical studies have shown that mass might be correlated with the shape of the Hydrogen α line (Bergemann et al., 2016); the strength of the Li I line at 6707 Å is sometimes also used as a proxy for age (Soderblom, 2010). Additional chemical clocks, such as [C/Fe] and [N/Fe] (Martig et al., 2016), [Y/Mg] (Spina et al., 2016), or chronometer pairs based on the radioactive species Th and U (Hill et al., 2017; Placco et al., 2017; Hansen et al., 2018a), have also been used.

One particularly important development during the past decade is related to the advent of large-scale spectroscopic surveys. Many surveys have been carried out on 2-, 4-, or even 8-m class telescopes, like the APOGEE and SDSS/SEGUE surveys (at the 2.5-m telescope at Apache Point Observatory), GALAH (at the 3.8-m AAT), and Gaia-ESO (at the 8-m VLT). The targets identified in low-resolution programs are often followed up at higher resolution with larger facilities, such as Keck and SUBARU (Beers and Christlieb, 2005). Future large-scale spectroscopic efforts include DESI, 4MOST, MOONS, WEAVE, PFS, and multi-object spectrographs at the GMT, TMT, and ELT, both in the optical and in the near-IR.

1.3 Modelling atmospheres and spectra of cool stars

Spectroscopy of cool stars greatly relies on models, in particular, on models of stellar atmospheres and model (synthetic) spectra. The models are usually computed in an ab-initio fashion, by consistently solving a set of equations to describe the energy balance and transfer in the atmospheres. The predicted observables include the stellar energy distribution (SED), photometric magnitudes, limb-darkening, spa-

tially resolved intensities, and detailed line profiles, which can be compared to the observations.

The classical 1-dimensional (1D) models have traditionally assumed several simplifying approximations, the assumption of hydrostatic equilibrium and Local Thermodynamic Equilibrium (LTE). Hydrostatic equilibrium describes the balance between gas pressure and gravitational force, $dP/dz = -g\rho(z)$, which can be regarded as the simplest form of the Navier-Stokes equations, ignoring any mass motions. To make the models more realistic, it is common to factor in other terms, such as radiative and turbulent pressures. The latter, $dP/dz \sim -\rho x v^2$, where v is the characteristic velocity. For energy conservation, the assumptions of flux constancy, i.e., no sources or sinks of energy, and radiative equilibrium (for the radiative flux calculations) are typically used. The convective energy transfer is treated using approximate recipes, such as the 'mixing-length theory'. The convective flux is $F_{\rm conv} \sim a_{\rm MLT}/H_p$, where $a_{\rm MLT}$ is the mixing-length parameter and $\rm H_p$ is the scale height, $H_p = -dr/dlnP$. In the hydrostatic approximation, H_p is proportional to $\sim P/\rho g$, the typical distance over which density drops by a factor of e. The mixing length describes the characteristic distance, travelled adiabatically (no exchange of energy with the environment), after which a mass element thermalises with the environment. LTE is a simple approximation, based on the Boltzmann and Saha formulae that describe the distribution of atoms among their internal energy states (excitation and ionisation). The Saha equation describing ionisation only holds in the limit of weak ionisation of the plasma, where Coulomb interactions between ions and electrons have no impact on the other charged particles, thus the 'screening' of the ionisation potential can be neglected.

These simplified 1D LTE models are broadly used, mainly because of their computational tractability. Huge grids of 1D LTE plane-parallel stellar atmospheres models have been computed already (Kurucz, 1993; Gustafsson et al., 2008). These models are also useful to explore the effect of individual parameters, such as opacities, on the energy balance.

Recent advances in the field focus on two major directions. New three-dimensional (3D) models (Collet et al., 2007; Nordlund et al., 2009; Freytag et al., 2012) deal with some major problems of the classical models, through the inclusion of full 3D hydrodynamics, at the expense of some simplifications related to radiative transfer. These models solve the compressible Euler equations for the conservation of mass, momentum, and energy, and exist in two variations: (a) the box-in-a-star model, which assume that the gravitation potential is constant ($dF/dz = -g$, and applied to solar-like stars), and (b) the star-in-a-box models, which include the entire star in the simulation box, and adopt a spherical gravitational potential with a softened

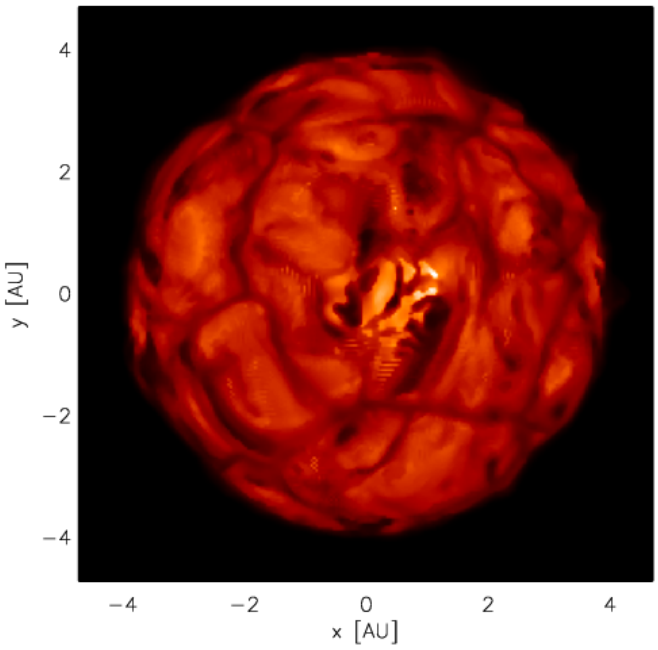

Figure 1.4 A 3D hydrodynamical simulation of a red supergiant star (Chiavassa et al. 2011).

$1/r$ profile (Freytag et al., 2002)[5]. The latter variant is needed when modelling pulsating stars and stars with very extended envelopes.

Recent studies of stellar convection have shown that the characteristic size of the granules at the surface scales with the pressure scale height (Schwarzschild, 1975; Freytag et al., 1997; Chiavassa et al., 2009; Trampedach et al., 2013; Tremblay et al., 2013). For red supergiants, H_p is huge, because of their very low densities at the surface and large radii, thus in the models of red supergiants enormous convective cells emerge (Chiavassa et al., 2011). The size of granules depends on wavelength. In the deeper layers, close to the depths where the 1.6μm (opacity minimum) continuum forms, the cells have a size of 1.8 to 2.5 AU in diameter. These cells evolve on the timescales of several years and penetrate deep into the star. In the outermost layers, at small optical depths, granules are of only a fraction of an AU in size, and vary on shorter timescales of less than a few months. For giants and supergiants, the photo-centre also changes because of variability, which has an

[5] The potential in the core region is softened to $1/\sqrt{(r^2 + a^2)}$, where a is the softening parameter.

impact on the accuracy and estimate of the parallaxes (Ludwig, 2006; Chiavassa et al., 2011).

Solar-like stars are covered by thousands of cells, with smaller diameters of only 10^3 km. The granulation pattern in theoretical models shows remarkable similarity when contrasted with spatially resolved observations of the Sun, not only in terms of the size of granules, but also intensity contrast, and variability, suggesting that the simulations are indeed offering a realistic description of the physics of these stars (Nordlund et al., 2009).

The 2D and 3D convective simulations have also been used to explore the mechanism of pulsations consistently with convection (Freytag and Höfner, 2008; Freytag et al., 2017). Early 1D simulations assumed a "sinusoidal piston", i.e., arbitrarily injected kinetic energy at the bottom to simulate the stellar pulsations (numerically, variable inner boundary conditions). In contrast, 3D radiative-hydrodynamics models show pulsations on the timescales of years, i.e., global periodic variations of the physical surface properties, which are usually referred to as "pulsations"[6]. These models also show that shocks, which are triggered by acoustic waves, move material from the inner regions to the outer regions, where dust forms and the radiative pressure on dust leads to stellar winds, consistent with observations of AGB stars.

Recently, it has become possible to perform detailed spectrum-synthesis calculations using 2D radiation-hydrodynamics (RHD) simulations of short-period Cepheids (Freytag et al., 2012). The RHD simulations are still limited in their treatment of radiative transfer by including grey opacities, but they are capable of producing self-excited oscillations due to the κ mechanism starting from initial hydrostatic conditions.

This enables a test of the validity of the quasi-static approximation, which has been used to study pulsating stars for decades. Intriguingly, new results employing RHD models show that the hydrostatic 1D model atmospheres may be used to provide unbiased estimates of stellar parameters, but only for the phases of maximum expansion and the beginning of the compression phase, corresponding to the photometric phases of 0.3 to 0.65 (where 0 is set to be the maximum light phase) (Vasilyev et al., 2017). It has also been shown that the long-standing problem of the "K-term", i.e., the putative residual negative line-of-sight velocity of the Galactic Cepheids (Parenago, 1945; Stibbs, 1956; Wielen, 1974; Pont et al., 1994; Nardetto et al., 2009) is simply the result of the convective blueshift (Vasilyev et al., 2017).

Another important ingredient of stellar atmosphere models is non-local thermodynamical equilibrium (NLTE). This term involves a large number of physical processes, which describe the various channels through which gas particles interacts with the radiation field, including excitation, ionisation, recombination, and charge

[6] Note that in these simulations it is difficult to distinguish radial from non-radial modes, since the change in volume is accompanied by a change in shape.

transfer (Barklem, 2016). NLTE calculations are now possible for very large atomic models, like those of neutral iron or cobalt (Bergemann et al., 2010). The available theoretical evidence indicates that the effects of deviations from LTE are typically not negligible, and vary both in sign and in magnitude. Whereas the spectral lines of the lighter elements, such as Li and O, usually exhibit negative NLTE effects (in the sense that NLTE abundances are lower than LTE ones), the optical lines of Fe-peak elements show positive effects. The situation is then reversed for the lines of even heavier species, like Cu, which again exhibit increasingly negative departures from LTE. These are mainly related to the abundance of the element, the ionisation potential of the ion in a given ionisation stage, and the excitation potential of the energy levels involved in the transition. Fe-peak elements are mostly affected by over-ionisation, whereas lighter species and the lines of singly-ionised (majority species) are mainly sensitive to resonance-line scattering. The analysis of NLTE diagrams, such as in Fig. 1.5, indicate that the NLTE effects are not completely random, but follow certain regularities, permitting predictions of the magnitude of the NLTE corrections even for the elements for which detailed calculations are not yet available. In particular, this behaviour suggests that the NLTE corrections for the optical Ni lines should be minor and positive, of ~ 0.05 dex. For heavier species with higher ionisation potentials, slightly negative NLTE effects are expected.

It is now also possible to combine 3D models and NLTE, either in the form of NLTE calculations with mean 3D (< 3D>) models (Osorio and Barklem, 2016; Bergemann et al., 2017a) or full 3D calculations, where radiative transfer is performed through 3D cubes of physical parameters (Amarsi and Asplund, 2017). The available evidence is still sparse, however, as comparison of mean 3D NLTE with 1D LTE, as well as with full 3D NLTE abundances, has only been performed for a limited number of chemical elements. The results indicate that, for the solar-like stars, full 3D NLTE, <3D> NLTE, and 1D NLTE results are consistent within the standard error of abundance determination (i.e., within 0.03 dex or even less), for Li, O, Na, Mg, Al, and Fe (Figure 1.5). Comparing this to the typical differences between 1D LTE and 1D NLTE estimates, which may differ by an order of magnitude, the available evidence suggests that full 3D NLTE calculations and NLTE calculations with averaged 3D models, as well the NLTE analysis with the standard 1D hydrostatic models, provide a solid basis for high-precision abundance diagnostics of late-type stellar spectra.

Finally, it is important to assess the accuracy of the models when applied to different regimes of the electromagnetic spectrum. For the Sun, there is sufficient evidence that chromospheric radiation transport plays an increasingly important role in the UV (Hauschildt et al., 1999; Hall, 2008; Linsky, 2017). The chromosphere is also visible in the cores of the strong lines, which is a particularly limiting factor in the infrared, where the number of spectral lines is far lower than at optical

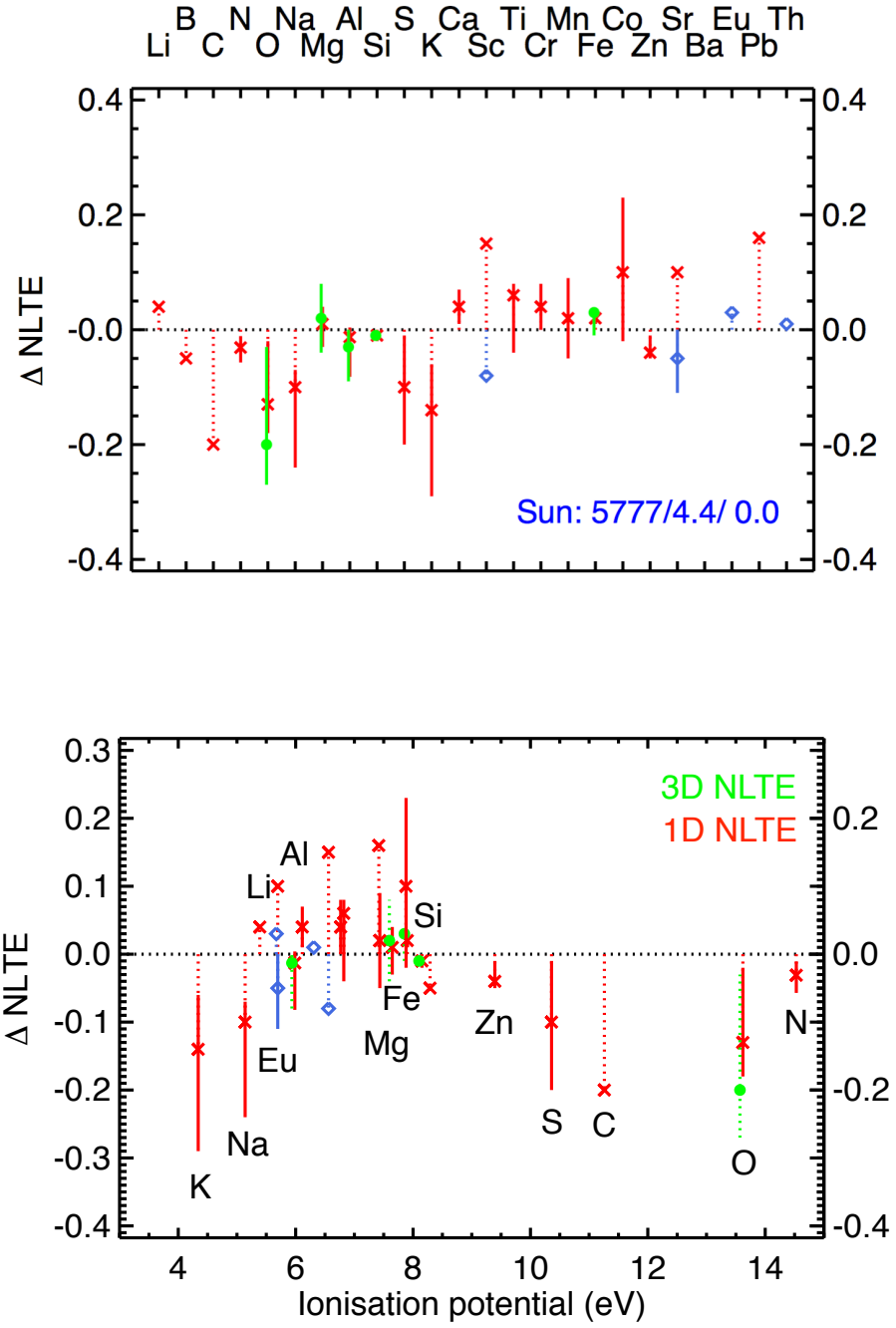

Figure 1.5 Differences between 1D NLTE and 1D LTE abundances (red for the lines of neutral species, blue for the lines of singly-ionised species), and 3D NLTE and 1D LTE (green) abundances for the Sun.

wavelengths. Whether the UV region is appreciably affected by the chromospheric radiation transport in stars other than the Sun is not yet well-understood. Observational evidence suggests that the chromosphere may affect even very metal-poor stars like HD 84937 ([Fe/H]= −2.0; Spite et al. 2017). Because of the absence of ab-initio chromospheric models for such stars, no conclusions on the accuracy of the UV diagnostics can yet be drawn.

1.4 A recap on stellar nucleosynthesis

Stars are the factories for all chemical elements beyond H and He in the Universe. Production of chemical elements occurs in stars of different types and different evolutionary phases, as different conditions are needed to reach the necessary temperatures and pressures to ignite specific nuclear reactions. Theoretical evidence, corroborated by meticulous observations of element abundances in SNe, AGB, and novae ejecta (José and Iliadis, 2011), indicate that there are several major groups of chemical elements that are co-produced under similar conditions, and thus can be used to trace specific production sites. These sites are described below, and are shown schematically on the cosmic abundance chart (Figure 1.6).

- Hydrogen (H, and Deuterium, D), He, a tiny amount of Li, and minuscule fractions of B and Be, are produced in Big Bang nucleosynthesis (BBN), during the first few minutes, when the temperature drops from 10^{32} K to 10^{9} K. Li production is still not entirely understood, and it is very sensitive to the photon-to-baryon number in the BBN (Steigman, 2007), which offers an interesting way to constrain the Big Bang models through observations of Li abundances in the oldest stars (Sbordone et al., 2010). Stellar models suggest that ^{7}Li can be destroyed by hot-bottom-burning (Lattanzio et al., 1996). Also, recent observations provide evidence for the production of Li in novae (Tajitsu et al., 2015). An important astrophysical puzzle is the depletion of Li in the oldest Galactic stars; the abundance of Li in their atmospheres is a factor of 3-4 less than what is expected from primordial nucleosynthesis (Fields, 2012). B and Be are produced mainly by cosmic ray spallation reactions. Some solar-like young stars show extreme under-abundance of Li and Be, which has been one of the prime puzzles in stellar evolution, but recent models with episodic bursty accretion and rotational mixing appear to resolve the puzzle (Viallet and Baraffe, 2012).
- Carbon, nitrogen, and oxygen are formed in intermediate-mass stars (AGB phase) and in massive stars. Carbon is produced via triple-α reactions during He burning, which has a low probability, and only works because of a fundamentally crucial Hoyle resonance, an excited energy state of ^{12}C, which matches exactly the interaction energy of ^{8}Be and an α-particle. Nitrogen can be formed in two

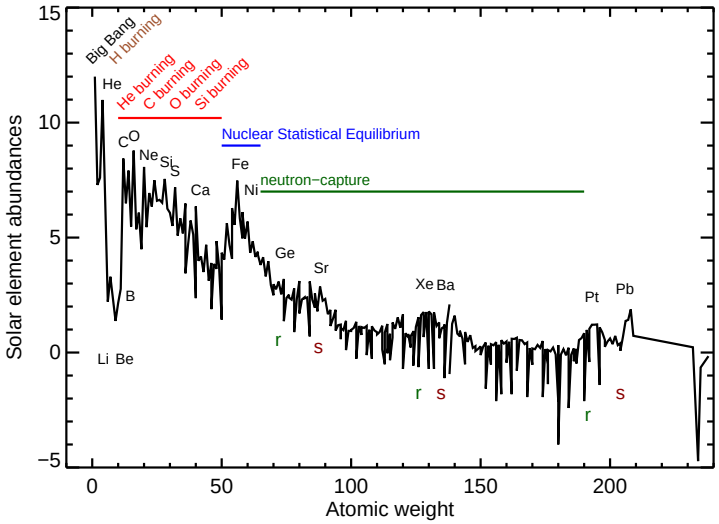

Figure 1.6 The abundances in the solar photosphere in the logarithmic scale (based on Lodders et al. 2009). The abundance of hydrogen is set to 12. The main element-production channels are indicated.

ways; if it is formed directly from He it is called primary nitrogen. This can take place in AGB or massive stars and requires a large degree of stellar rotation

and mixing (Spite et al., 2005; Chiappini et al., 2005). If, on the other hand, N is formed at the expense of C and O in the CNO cycle, it is referred to as secondary N (Spite et al., 2005).

- The production of alpha elements goes on via a sequence of ^{4}He captures on nuclei. The α-capture on ^{12}C makes stable ^{16}O, releasing some energy. This is then followed by the α-ladder, producing stable isotopes of Mg, Si, S, Ca, and unstable isotopes ^{44}Ti (decays to ^{44}Ca), ^{48}Cr (decays to ^{48}Ti), ^{52}Fe (decays to ^{52}Cr), and ^{56}Ni. The latter has the maximum binding energy per nucleon and decays to the dominant isotope of iron, ^{56}Fe.
- The odd-Z elements ^{23}Na and ^{27}Al are produced during the carbon- and neon-burning phases in intermediate-mass and massive stars, $M > 3\ M_{\odot}$. They are thought to be so-called 'secondary' nuclei, requiring pre-existing neutron-rich seed nuclei (Gehren et al., 2006).
- Fe-peak elements require very high temperatures and pressures for their production. Furthermore, neutron-rich (odd-Z) elements, like Mn and Co, also depend on the neutron enrichment. These conditions are usually satisfied during the late stages of the evolution of massive stars (which are then composed of multiple shells, in which nuclear burning takes place) and during explosions. Recent models of SN Ia explosions (Seitenzahl et al., 2013; Seitenzahl and Townsley, 2017) indicate that the production of Mn is an extremely sensitive tracer of Type Ia SNe. A fraction of Ti and Cr is produced during hydrostatic O burning. Heavier elements are produced in explosive conditions in supernovae, when the outward propagating shock wave heats the matter to sufficiently high temperatures necessary for the production of these high-Z species. Some species are produced by incomplete Si burning, such as Cr and Mn, while others are produced in the region of complete Si burning (e.g., Co) and α-rich freeze-out from nuclear statistical equilibrium (Thielemann et al., 2007). The difference between the two lies essentially in the peak temperature in the burning layer. Incomplete Si burning typically occurs at $4 \cdot 10^9$ K < T < $5 \cdot 10^9$ K, whereas compete Si burning occurs at T > $5 \cdot 10^9$ K (Thielemann et al., 2007).
- Thermonuclear fusion does not produce elements beyond Fe – Ni. The reason is that charged-particle reactions past ^{56}Ni are endoergic, i.e. they no longer produce energy, but consume it. Thus, most elements heavier than iron form by capturing neutrons onto heavy existing isotopes and subsequent β-decays. Only very few proton-rich nuclei are produced by a *p*-process [7], which may be associated with core-collapse supernovae[8] or SN Ia.

There are two main channels through which the elements beyond the Fe peak

[7] Only 35 stable p-nuclei exist (Travaglio et al., 2018).

[8] This could be a νp-process taking place in core-collapse supernovae as proposed by, e.g., Fröhlich et al. (2006).

can be formed, either through a slow neutron-capture (*s*-) process, where the capture rate is much longer than the subsequent beta-decay rate, or the rapid neutron-capture (*r*-) process, where the captures happen much faster than the decay, driving the process far from the so-called valley of stability.

- The *s*-process is a secondary process, requiring pre-existing seed nuclei, and it typically takes place in AGB stars, which burn H and He in shells. The He-rich layer, which separates the two shells, hosts ^{13}C-rich pockets, which form through captures of protons from the convective envelope onto ^{12}C nuclei. Then, the reaction ^{13}C(α,n)^{16}O produces free neutrons, which are captured onto existing seeds, typically Fe-peak nuclei, creating nuclei with atomic numbers $A \sim 90-205$. This process is thought to be responsible for the main *s*-process component. In more massive stars, M> 15 $M_{\odot}$, *s*-process nucleosynthesis can take place through the ^{22}Ne(α,n) ^{25}Mg reaction, at higher temperatures and densities (Frischknecht et al., 2016). This process is thought to produce the weak *s*-process component ($A < 90$). None of these processes can be observed directly, and to date there remain many unknowns associated with them, where the size of the ^{13}C-pockets remain one of the largest uncertainties. Recent studies detected the radioactive Tc which is only produced by the *s*-process in pulsating AGB stars (Merrill, 1952; Neyskens et al., 2015).
- Approximately half of the heavy elements are, however, not formed by the *s*-process, but are attributed to the *r*-process, a primary process that can form the heaviest isotopes starting out with just protons and many neutrons. This means that no pre-existing heavy isotope is needed in this process. The *r*-process requires extreme conditions, such as very high neutron densities ($> 10^{25}$cm^{-3}), high temperatures, high entropies, and fast expansion of the explosion. Previously, the *r*-process was thought to be primarily associated with core-collapse SNe explosions. However, recent 2D SNe models have shown that the 9-11M$_{\odot}$ SNe are not sufficiently neutron rich to produce elements heavier than Sn ($Z = 50$) (Wanajo et al., 2011).

  Recent observations of the 'kilonova' SSS17a (Drout et al., 2017; Kasen et al., 2017; Pian et al., 2017; Shappee et al., 2017; Smartt et al., 2017) provide strong indications that the *r*-process is likely to be hosted by the merger of two neutron stars (NSM), an event that has recently received a great deal of attention because of its association with the gravitational wave detection GW170817 by the advanced LIGO-VIRGO collaboration. NSMs are extremely rich in neutrons and can easily host the *r*-process. A merger of two neutron stars emits gravitational waves, produces a kilonova event (Metzger et al., 2010), and powers a short gamma ray burst. The afterglow of a kilonova is powered by the radioactive decay of unstable heavy isotopes, and a boost in the abundance of lanthanides detectable in the near-IR is expected (Tanvir et al., 2013; Martin et al., 2015).

However, one should keep in mind that neutron stars are also the endpoints of the evolution of massive stars, and so far it has not been possible to separate the contribution of heavy element material from rare core-collapse SNe explosions or ejecta of a NSM based on observations (Thielemann et al., 2017). Massive supernovae can also form the *r*-process elements, provided they have strong magnetic fields and explode asymmetrically with jets (Nishimura et al., 2017; Mösta et al., 2017). This needs to be probed in more detail with refined models and observations.

1.5 Stellar populations and Galactic Chemical Evolution (GCE)

The chemical abundance measurements in stars, as well as theoretical studies of element production, have an important application in astrophysics – studies of the chemical evolution of stellar populations and galaxies.

As massive stars evolve faster, their ejecta will pollute the interstellar medium (ISM) earlier (on shorter time scales) than is the case for lower-mass stars. The latter take longer to evolve and to eject their processed material. Therefore, lower-mass stars will experience a time delay with respect to more massive objects, which end their lives as SNe, leaving behind neutron stars, black holes, or nothing at all. Thus, by observing stars with different masses and ages, we can study the chemical evolution of galaxies, and, hence, the associated processes that influenced their formation, such as mergers, infall and outflows, galactic winds, the initial mass function, and star-formation activity (Tinsley, 1979; Lacey and Fall, 1983; Goetz and Koeppen, 1992). On the other hand, old stars, which are also expected to be the most metal-poor ones, probe the first heavy element pollution of the ISM after the Big Bang, and they are excellent testbeds of stellar yields, the first initial mass function, and early stellar evolution (Bromm and Larson, 2004; Matteucci and Calura, 2005).

A few observational trends stand out clearly when we study Galactic Chemical Evolution. Stars with metallicity below [Fe/H]~ -2 show a large star-to-star abundance scatter in neutron-capture elements, such as Ba, compared to elements like Mg, which exhibit little scatter (Figure 1.8). Since most of these very metal-poor stars are halo stars, when identified by their space motions (kinematics) [9], this observation provides constraints on the Galactic halo formation. In particular, the heavy-element scatter may indicate that the Galaxy was inhomogeneous in the early stages, and the halo could have hosted transient star-forming regions

[9] Halo stars exhibit a wide range of orbital eccentricities, including low and high eccentricity. Compared to the disc stars, which have exclusively low-eccentricity orbits, halo stars also have much larger velocity dispersions.

that were dense and sufficiently massive to sustain prolonged self-enrichment by Type II and Type Ia SNe (Gilmore and Wyse, 1998; Karlsson, 2005; Karlsson and Gustafsson, 2005).

The scatter in *s*-process elements in stars with [Fe/H] < -2 may also indicate that the massive objects might have ejected different amounts of elements, i.e., having yields that are dependent on mass and metallicity (Maeder, 1990). Then, the fact that the scatter decreases at metallicities above [Fe/H]≈ -2 is consistent with the general enrichment dominated by several distinct nucleosynthesis channels, and reflects the background metallicity level. The relative pollution by an individual object becomes less significant as the base metallicity level increases. This is best seen in the distributions of, e.g., elements produced by the *s*- and *r*-process. The change in scatter could also be related to the onset of AGB pollution, as these stars will have had sufficient time to evolve and eject material rich in C, N, and *s*-process elements (Busso et al., 1999).

Under closer inspection, observations suggest that the Galactic halo population is even more complex. It has now been firmly established that galaxies form through mergers and accretion of sub-halos (Searle and Zinn, 1978; White and Frenk, 1991; Bullock and Johnston, 2005). This implies not only that some scatter in chemical abundances of the halo stars is expected, but also that chemical-abundance diagrams may contain specific 'features', indicating stellar populations which were not formed in-situ in the Milky Way, but were added to our galaxy over time. The known dwarf galaxies exhibit a very large range of star formation histories (Tolstoy et al., 2009; Kirby et al., 2011; Leaman, 2012). Recent observations indicate that the halo indeed has a metal-rich ([Fe/H] ~ -1) stellar component, which hosts low-[α/Fe] stars (Nissen and Schuster, 1997, 2010), suggesting their origin in dwarf galaxies. The metal-rich part of the halo and the thick-disc stars overlap in metallicity, with the thick disc extending to [Fe/H] ~ -1.8. However, in contrast to the thick-disc population, the halo stars show an inverse correlation between [Fe/H] and α/Fe (Bergemann et al., 2017b); the slope of the trend line is important for chemical-evolution models.

The structure of the Galactic halo is still a matter of a debate. Carollo et al. (2007, 2010), Beers et al. (2012), and others since, have argued that "the halo" comprises both inner-halo and outer-halo populations of stars, based on their observed spatial distribution, kinematics, and chemical abundances (the inner-halo population peaking at metallicity [Fe/H] ~ -1.6; the outer-halo population peaking at [Fe/H] ~ -2.2). This evidence is important, because the populations mark different eras of formation, and differences in the mass distributions of the sub-galactic fragments (mini-halos) that merged or were accreted during their formation. Numerical galaxy-formation simulations also lend support to this view (Font et al., 2011; McCarthy et al., 2012; Tissera et al., 2013, 2014, 2018).

However, some have questioned this interpretation (Schönrich et al., 2011; Deason et al., 2013; Schönrich et al., 2014), suggesting that the secondary (retrograde rotating) halo component should be much weaker, if present. In this context, it is interesting that the Gaia DR2 collaboration has reported an intriguing duality in the CMD plane of kinematically selected halo stars, suggesting two components with [Fe/H] of -1.3 and -0.5 (Gaia Collaboration et al., 2018). At least one of these could be related to the inner-halo population described above, but more evidence in the form of ages and detailed chemical abundances will be needed to understand the origin of this structure.

Generally, the interpretation of chemical abundance-age-kinematics diagrams in the context of Galaxy formation scenarios is non-trivial. Although the overall abundances of heavy elements generally increases with time, detailed observations show that the metallicity of stars does not uniquely correlate with age, neither during the Galactic halo nor during disc formation (Holmberg et al., 2009; Bergemann et al., 2014). Galaxy-formation simulations suggest that the oldest stars are expected to be found in the Galactic bulge, the most metal-rich component of the Milky Way (White and Springel, 2000; Brook et al., 2007; Starkenburg et al., 2017; Griffen et al., 2018).

The apparent distribution of stars in the chemical-abundance plane is, however, highly sensitive to the selection function of the observational program (Bergemann et al., 2014; Thompson et al., 2018). "Mono-metallic" or "mono-abundance" stellar populations, i.e., groups of stars exhibiting similar abundances, do not necessarily imply that they are co-eval, or even formed within the same Galactic component. Conversely, stars formed in the halo, in the disc, or in the bulge, do not possess a well-defined characteristic signature in the chemical-abundance plane, and even less so in kinematics. In particular, and in contrast to the surface chemical composition of unevolved stars, stellar kinematics does change after stellar birth (Binney and Lacey, 1988). Stars experience dynamical disturbances in the Galaxy that changes their orbits, and this kinematical re-arrangement makes it difficult to tag stars and identify their parent population. Stars formed in the Galactic centre can be relocated into the outer bulge or inner halo (El-Badry et al., 2018), those formed in the disc plane acquire large altitudes above the plane (Laporte et al., 2017; Bergemann et al., 2018), and disc stars themselves experience radial migration via scattering of giant molecular clouds and transient spiral arms (Sellwood and Binney, 2002; Schönrich and Binney, 2009a,b).

More metal-rich stars, mostly members of the disc, show another interesting correlation: The relative abundances of their $\alpha-$elements, [α/Fe], indicate a break at [Fe/H]~ -1. This is commonly referred as a *knee*, and is thought to arise because of the onset of SN Ia pollution (Matteucci and Greggio, 1986). SN Type Ia events result from mass transfer in a binary system of low mass stars. They have a typ-

ical time delay of $\sim$ 1 Gyr, although there is extragalactic evidence for a fast SN Ia channel (Mannucci et al., 2006). SN Ia produce substantial amounts of Fe-peak elements, but very little $\alpha-$elements, resulting in the downward trend (Fig. 1.7 and 1.8). The proposed dual structure of the Galactic disc, which is seen in the [α/Fe] vs. [Fe/H] in some elements, but not in the others, is still a matter of debate (Lee et al., 2011; Mikolaitis et al., 2014; Bergemann et al., 2014). Bensby et al. (2014) found the bimodal distribution in [Ti/Fe], but not in [Mg/Fe], whereas Hawkins et al. (2016) observe bi-modality in [Mg/Fe] but not in [Ti/Fe]. The old unsettled problem of whether the thick disc is a stand-alone population with a formation history different from that of the thin disc (Chiappini et al., 1997) is, in turn, complicated by the apparent complex structure of the former being not a monolithic population (Spagna et al., 2010; Curir et al., 2012; Schönrich and McMillan, 2017). Volume complete, statistically significant samples of stars need to be analysed in high-quality spectra and with updated models, to control for systematic errors, and settle this debate.

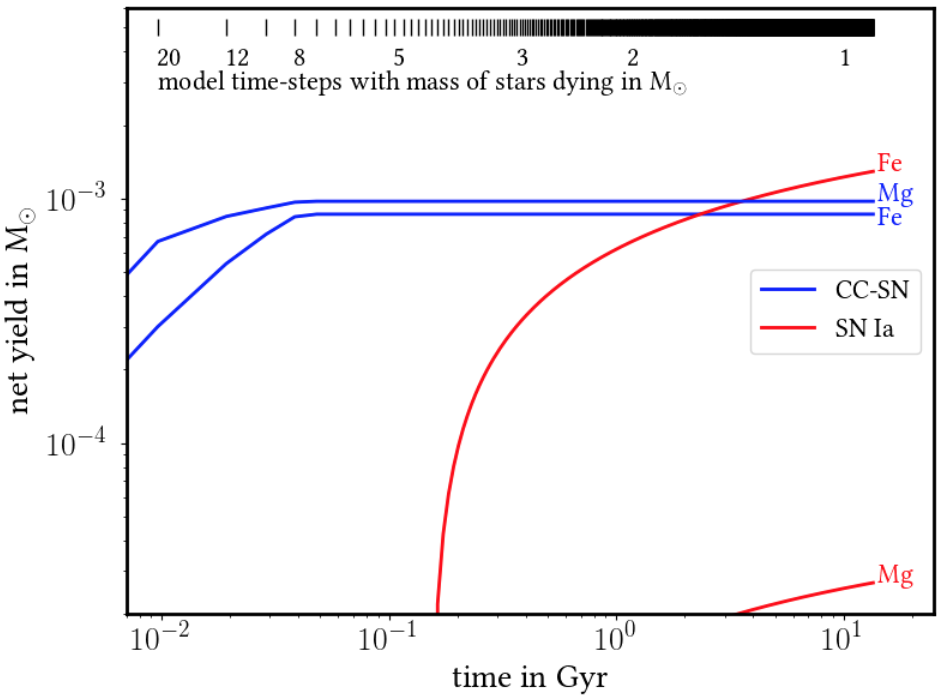

Figure 1.7 The evolution of the net yields of Mg and Fe in a simple stellar population (adapted from Rybizki et al. 2017).

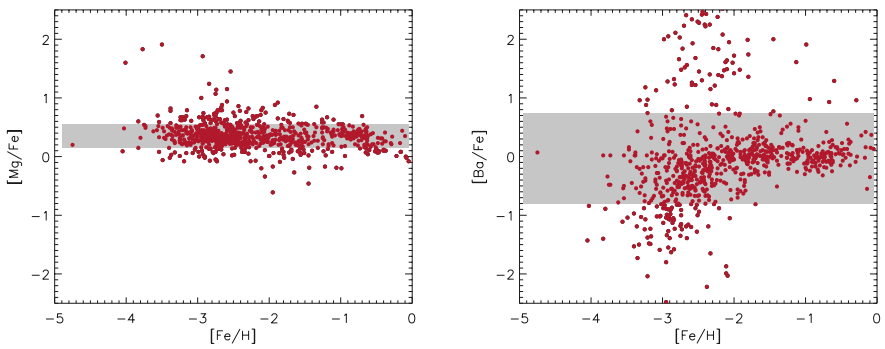

Figure 1.8 Left panel: [Mg/Fe] vs [Fe/H], right panel: [Ba/Fe] vs [Fe/H]. Note the difference in star-to-star scatter as indicated by the standard deviation around the mean (grey shaded region). Data from the Frebel (2010) compilation. Figure adopted from Hansen et al. (2014).

1.5.1 Old and unique chemical tracers

Among the low-metallicity stars in the halo, there exist a number of stars with particularly important abundance patterns, which are shaping our view of the origin of the elements.

The star CS 22982-052, one of the most strongly *r*-process-enhanced stars (an *r*-II star, following Beers and Christlieb 2005, with [Eu/Fe] > +1.0), was analysed most recently by Sneden et al. (2003). Up until 2013, this was the star for which we had the most complete abundance information after the Sun. However, Siqueira Mello et al. (2013), based on both HST- and ground-based high-resolution spectra, analysed the *r*-II star CS 31082-001, and obtained measurements for a total of almost 70 stable elements in the periodic table (including the "jewelry store" elements silver, gold, and platinum, as well as the radioactive species thorium and uranium). Although these stars exhibit essentially identical elemental-abundance patterns among the heavy elements from Ba to Hf (matching a scaled-solar *r*-process distribution), they differ dramatically in their [Th/Eu] abundance ratios, a phenomenon referred to as the "actinide boost" (see, e.g., Mashonkina et al.

2014). Roughly 30% of *r*-process-enhanced stars exhibit the actinide boost, which may provide a fundamental clue to the origin of the *r*-process. Over the past few decades, a total of $\sim 25 - 30$ *r*-II stars have been identified. This number is expected to dramatically increase in the near future due to dedicated survey efforts now underway, e.g., the *R*-Process Alliance effort (Hansen et al., 2018b), whose goal is to bring the number of known *r*-II stars up to on the order of 100 or more. Such large, "statistical" samples, are required to search for the subtle elemental-abundance signatures that may be used to differentiate different astrophysical sites of the *r*-process.

By way of contrast, there also exist stars that appear highly deficient in their light and heavy *r*-process elements, relative to a scaled-solar pattern. HD 88609 and HD 122563 are two such stars (Honda et al., 2007), which have been used to support the operation of a "weak" or "limited" *r*-process, decoupled from the "main" *r*-process (Hansen et al. 2012, 2014, Frebel subm).

To date, the most Fe-poor star yet found was discovered by Keller et al. (2014). This CEMP star is so Fe-poor that it only has an upper limit of [Fe/H] < -7.5. Comparison to yield predictions from supernovae (e.g., Heger and Woosley 2002) showed that the chemistry matched that of the ejecta from a $60 M_{\odot}$ Type II SN. However, later 3D and NLTE corrections to both molecular and atomic line abundances indicated a slightly higher metallicity, as well as a less massive progenitor (Bessell et al., 2015; Nordlander et al., 2017). Another interesting, hyper metal-poor star, SDSS J102915+172927, was recognized a few years earlier by Caffau et al. (2011), from high-resolution spectroscopic follow-up of extremely metal-poor turnoff stars identified in the Sloan Digital Sky Survey. This star is unique in the sense that it has [Fe/H] ~ -5, but unlike all other such extreme stars, the star appears to lack a signature of carbon enrichment (however, only weak upper limit on [C/Fe] has been as yet reported). Recently, additional ultra, hyper, and mega ([Fe/H] < -6) metal-poor TO stars from SDSS have been reported by Aguado et al. (2018), and references therein, all of which exhibit carbon enhancement (or have upper limits on [C/Fe]), indicating that they are CEMP stars.

Significant fractions of very metal-poor stars are in fact known to be CEMP stars. These stars can be further divided into sub-classes based on their neutron-capture elemental-abundance patterns. CEMP-*s* stars are the most populated sub-class, where the elements representing the slow neutron-capture process are prominent. At least 80% of the CEMP-*s* stars are binaries (Starkenburg et al., 2013; Hansen et al., 2016b), and almost certainly are associated with mass-transfer events from a former AGB companion. However, several stars in this sub-class are suspected to be single stars, which might be explained by massive-star pollution (Choplin et al., 2017) of the natal cloud from which the low-mass star observed today formed. In contrast, the CEMP-no stars are characterized by a lack of neutron-capture over-

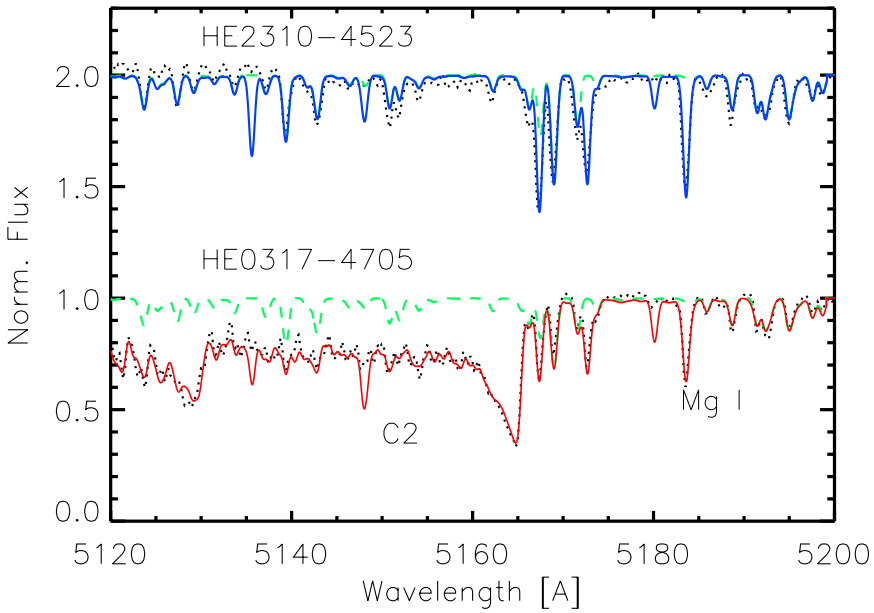

Figure 1.9 Observations of two stars (black dots) with similar stellar parameters (and [Fe/H]=-2.5) but very differing chemical composition. Top: HE 2310-4523 compared to synthetic spectra (blue line) with [C/Fe] = +0.2 and [Mg/Fe] = +0.25 (Hansen et al. 2016), bottom: HE 0317-4705 and synthetic spectra (red line) with [C/Fe] = +1.4, [Mg/Fe] = +0.5 (Hansen et al. subm.). The green dashed line represents no C and no Mg.

abundances. A number of lines of evidence point to their formation very early in the history of the Universe, and indeed some CEMP-no stars may well represent bona-fide second-generation stars that have locked up the nucleosynthesis products of the very first (massive) stars (see Hansen et al. 2016a, and references therein). A handful of stars to date have been identified as CEMP-*r* stars, which, in addition to their carbon-enhancement, exhibit strong over-abundances of *r*-process elements (interestingly, this class includes the canonical *r*-II star CS 22892-052). Their origin is still very much under discussion. Finally, a hybrid class, known as CEMP-r/s stars, includes carbon-enhanced stars with both *r*- and *s*-process elemental-abundance signatures present in their spectra. At first, it proved difficult to explain how both the *r*- and *s*-process enriched material got mixed into these stars, however, recent models have shown that a nucleosynthetic process, the so-called intermediate neutron-capture process (*i*-process), which may operate in AGB or massive stars, might explain this abundance pattern (Dardelet et al., 2014; Hampel et al., 2016; Clarkson et al., 2018).

Although the signature of increasing fractions of CEMP stars with decreasing [Fe/H] has been recognized for many years (Beers and Christlieb 2005, and references therein), the most recent evaluation of their frequencies have been revised upward by as much as a factor of two, compared with the previous result (Lee et al., 2013)[10]. Two CEMP classes can be distinguished in a relatively simple way. Spite et al. (2013) and Bonifacio et al. (2015) demonstrated that the two dominant classes of CEMP stars have different enhancements of absolute C abundances ($A(\mathrm{C}) = \log\epsilon(\mathrm{C}) = \log\ (N_C/N_H) + 12$,). The CEMP-*s* stars exhibit a high level of A(C), mainly owing to C-rich material being transferred in a binary system, while the CEMP-no stars (typically not binaries) have lower A(C).

Yoon et al. (2016) demonstrated that the morphology of the A(C)-[Fe/H] space is richer still, separating out three groups of CEMP stars, the Group I stars comprising CEMP-*s* stars, and the Group II and Group III stars comprising CEMP-no stars with apparently different progenitors ors and/or enrichment histories. Yoon et al. further showed that CEMP-*s* and CEMP-no stars can be distinguished based on medium-resolution spectroscopic measurement of A(C) alone, with a success rate commensurate with that obtained from high-resolution spectroscopic measurement of Ba. From application of this approach, one can clearly see the very different behaviours of CEMP-no and CEMP-*s* stars in the revised frequency diagram (Fig. 1.10). Comparison of these derived frequencies with predictions from

[10] This revision arises for two primary reasons. First, CEMP stars near the TO were under-counted in the Lee et al. (2013) study, due to the diminished strength of the CH $G-$band for stars with $T_{\rm eff} > 5750$ K, and corrections needed to be applied to cooler RGB stars to account for the effect of carbon dilution from first dredge-up. The Yoon et al. 2018 (subm.) study includes only SG and RGB stars, with the correction of Placco et al. (2014) applied.

population synthesis and numerical galaxy assembly models should prove illuminating.

1.6 Conclusions and future outlook

We have endeavoured to provide a brief overview of an extremely broad set of topics, and in truth have only brushed the surface. Many of the fields discussed in the present chapter are advancing rapidly, and will remain vibrant for a long time. It is easy to forget that no more than a century has passed since humans came to understand that the Milky Way is but one of perhaps 100 billion galaxies in the Universe, and that nuclear fusion powers individual stars over their lifetimes, no matter how brief or how long. As of this writing, the Gaia mission is making its second public data release, with new, precise, information on distances, proper motions, and spectral energy distributions for more than a billion stars in the Galaxy, and radial velocities for many millions of the brighter stars. Significantly more detailed information will follow once the full dataset is acquired and distributed. This represents the beginning of a new era, where fundamental information for the stars of the Milky Way will enable researchers to confront outstanding issues with a level of detail that was not imaginable a few decades ago.

Our ability to model many aspects of the evolution of stars, in particular those which can be used to infer the nature of the earliest generations born in the Universe, is still in relative infancy. Present and future massive photometric and spectroscopic surveys of resolved stellar populations in the Milky Way will no doubt spur these modelling efforts to take on even greater challenges. The success of these efforts depends crucially on the contributions from astronomers and physicists who are only now beginning their careers, so they must be encouraged and nurtured in order to carry this quest for understanding to the next level.

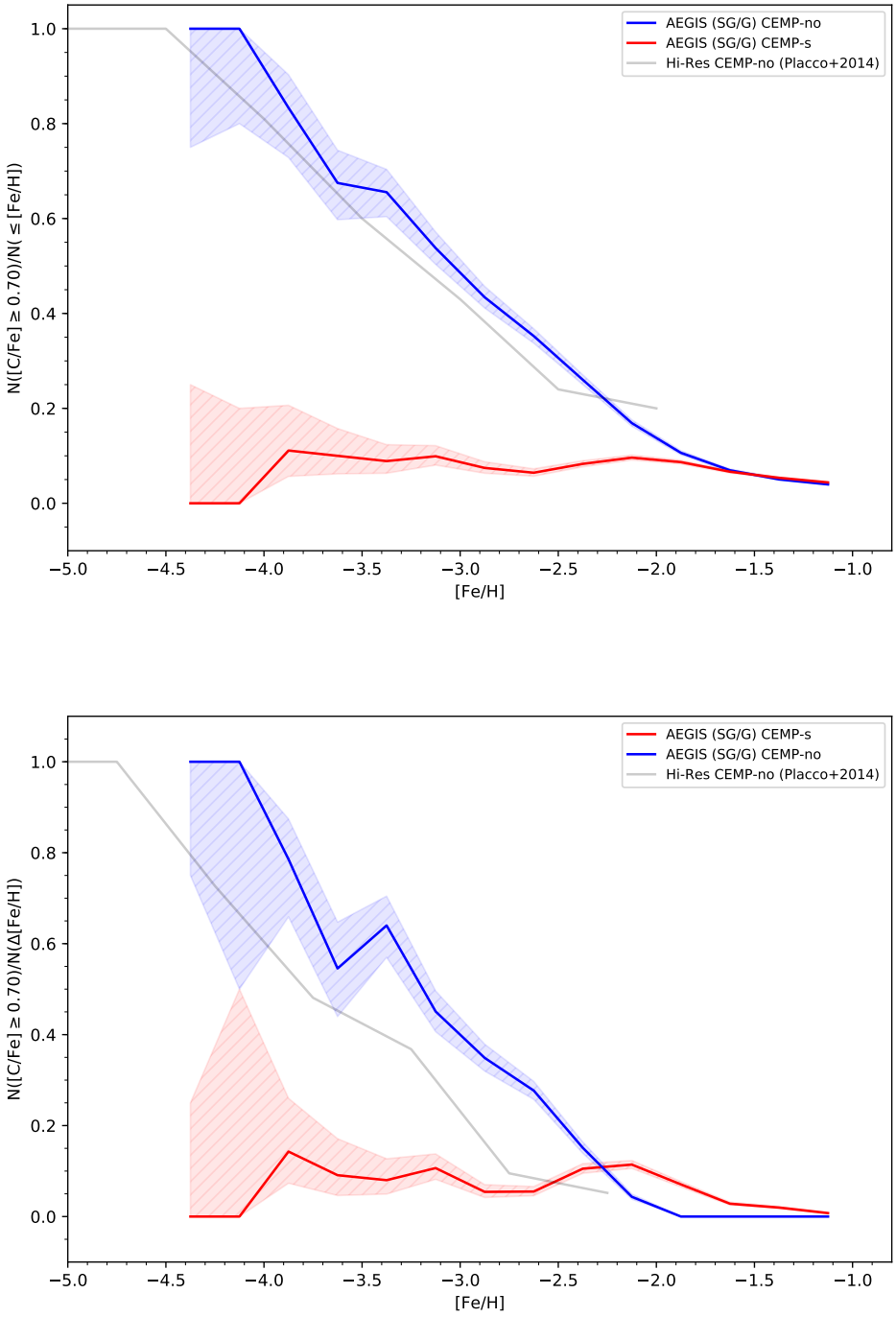

Figure 1.10 The cumulative and differential CEMP frequencies, as a function of [Fe/H], plotted separately for CEMP-no and CEMP-*s* stars, classified from medium-resolution spectroscopy. The light grey line indicates the frequencies of CEMP-no stars for a sample of stars with available high-resolution spectroscopic information, from Placco et al. (2014). (Figure adopted from Yoon et al. 2018, subm.).

References

Aguado, D. S., Allende Prieto, C., González Hernández, J. I., and Rebolo, R. 2018. J0023+0307: A Mega Metal-poor Dwarf Star from SDSS/BOSS. *ApJ*, **854**(Feb.), L34.

Allende Prieto, C., Lambert, D. L., Tull, R. G., and MacQueen, P. J. 2002. Convective Wavelength Shifts in the Spectra of Late-Type Stars. *ApJ*, **566**(Feb.), L93–L96.

Amarsi, A. M., and Asplund, M. 2017. The solar silicon abundance based on 3D non-LTE calculations. *MNRAS*, **464**(Jan.), 264–273.

Asplund, M., Grevesse, N., Sauval, A. J., and Scott, P. 2009. The Chemical Composition of the Sun. *ARA&A*, **47**(Sept.), 481–522.

Barklem, P. S. 2016. Accurate abundance analysis of late-type stars: advances in atomic physics. *A&A Rev.*, **24**(May), 9.

Beers, T. C., and Christlieb, N. 2005. The Discovery and Analysis of Very Metal-Poor Stars in the Galaxy. *ARA&A*, **43**(Sept.), 531–580.

Beers, T. C., Carollo, D., Ivezić, Ž., An, D., Chiba, M., Norris, J. E., Freeman, K. C., Lee, Y. S., Munn, J. A., Re Fiorentin, P., Sivarani, T., Wilhelm, R., Yanny, B., and York, D. G. 2012. The Case for the Dual Halo of the Milky Way. *ApJ*, **746**(Feb.), 34.

Bensby, T., Feltzing, S., and Oey, M. S. 2014. Exploring the Milky Way stellar disk. A detailed elemental abundance study of 714 F and G dwarf stars in the solar neighbourhood. *A&A*, **562**(Feb.), A71.

Bergemann, M., and Gehren, T. 2008. NLTE abundances of Mn in a sample of metal-poor stars. *A&A*, **492**(Dec.), 823–831.

Bergemann, M., Pickering, J. C., and Gehren, T. 2010. NLTE analysis of CoI/CoII lines in spectra of cool stars with new laboratory hyperfine splitting constants. *MNRAS*, **401**(Jan.), 1334–1346.

Bergemann, M., Lind, K., Collet, R., Magic, Z., and Asplund, M. 2012. Non-LTE line formation of Fe in late-type stars - I. Standard stars with 1D and ¡3D¿ model atmospheres. *MNRAS*, **427**(Nov.), 27–49.

Bergemann, M., Ruchti, G. R., Serenelli, A., Feltzing, S., Alves-Brito, A., Asplund, M., Bensby, T., Gruyters, P., Heiter, U., Hourihane, A., Korn, A., Lind, K., Marino, A., Jofre, P., Nordlander, T., Ryde, N., Worley, C. C., Gilmore, G., Randich, S., Ferguson, A. M. N., Jeffries, R. D., Micela, G., Negueruela, I., Prusti, T., Rix, H.-W., Vallenari, A., Alfaro, E. J., Allende Prieto, C., Bragaglia, A., Koposov, S. E., Lanzafame, A. C., Pancino, E., Recio-Blanco, A., Smiljanic, R., Walton, N., Costado, M. T., Franciosini, E., Hill, V., Lardo, C., de Laverny, P., Magrini, L., Maiorca, E., Masseron, T., Morbidelli, L., Sacco, G., Kordopatis, G., and Tautvaišienė, G. 2014. The Gaia-ESO Survey: radial metallicity gradients and age-metallicity relation of stars in the Milky Way disk. *A&A*, **565**(May), A89.

Bergemann, M., Serenelli, A., Schönrich, R., Ruchti, G., Korn, A., Hekker, S., Kovalev, M., Mashonkina, L., Gilmore, G., Randich, S., Asplund, M., Rix, H.-W., Casey, A. R., Jofre, P., Pancino, E., Recio-Blanco, A., de Laverny, P., Smiljanic, R., Tautvaisiene, G., Bayo, A., Lewis, J., Koposov, S., Hourihane, A., Worley, C., Morbidelli, L., Franciosini, E., Sacco, G., Magrini, L., Damiani, F., and Bestenlehner, J. M. 2016. The Gaia-ESO Survey: Hydrogen lines in red giants directly trace stellar mass. *A&A*, **594**(Oct.), A120.

Bergemann, M., Collet, R., Amarsi, A. M., Kovalev, M., Ruchti, G., and Magic, Z. 2017a. Non-local Thermodynamic Equilibrium Stellar Spectroscopy with 1D and ¡3D¿ Models. I. Methods and Application to Magnesium Abundances in Standard Stars. *ApJ*, **847**(Sept.), 15.

Bergemann, M., Collet, R., Schönrich, R., Andrae, R., Kovalev, M., Ruchti, G., Hansen, C. J., and Magic, Z. 2017b. Non-local Thermodynamic Equilibrium Stellar Spectroscopy with 1D and ¡3D¿ Models. II. Chemical Properties of the Galactic Metal-poor Disk and the Halo. *ApJ*, **847**(Sept.), 16.

Bergemann, M., Sesar, B., Cohen, J. G., Serenelli, A. M., Sheffield, A., Li, T. S., Casagrande, L., Johnston, K. V., Laporte, C. F. P., Price-Whelan, A. M., Schönrich, R., and Gould, A. 2018. Two chemically similar stellar overdensities on opposite sides of the plane of the Galactic disk. *Nature*, **555**(Mar.), 334–337.

Bessell, M. S., Collet, R., Keller, S. C., Frebel, A., Heger, A., Casey, A. R., Masseron, T., Asplund, M., Jacobson, H. R., Lind, K., Marino, A. F., Norris, J. E., Yong, D., Da Costa, G., Chan, C., Magic, Z., Schmidt, B., and Tisserand, P. 2015. Nucleosynthesis in a Primordial Supernova: Carbon and Oxygen Abundances in SMSS J031300.36-670839.3. *ApJ*, **806**(June), L16.

Binney, J., and Lacey, C. 1988. The diffusion of stars through phase space. *MNRAS*, **230**(Feb.), 597–627.

Bonifacio, P., Caffau, E., Spite, M., Limongi, M., Chieffi, A., Klessen, R. S., François, P., Molaro, P., Ludwig, H.-G., Zaggia, S., Spite, F., Plez, B., Cayrel, R., Christlieb, N., Clark, P. C., Glover, S. C. O., Hammer, F., Koch, A., Monaco, L., Sbordone, L., and Steffen, M. 2015. TOPoS . II. On the bimodality of carbon abundance in CEMP stars Implications on the early chemical evolution of galaxies. *A&A*, **579**(July), A28.

Bono, G., Caputo, F., and Santolamazza, P. 1997. Evolutionary scenario for metal-poor pulsating stars. I. Type II Cepheids. *A&A*, **317**(Jan.), 171–177.

Bromm, V., and Larson, R. B. 2004. The First Stars. *ARA&A*, **42**(Sept.), 79–118.

Brook, C. B., Kawata, D., Scannapieco, E., Martel, H., and Gibson, B. K. 2007. The Spatial Distribution of the Galactic First Stars. II. Smoothed Particle Hydrodynamics Approach. *ApJ*, **661**(May), 10–18.

Bullock, J. S., and Johnston, K. V. 2005. Tracing Galaxy Formation with Stellar Halos. I. Methods. *ApJ*, **635**(Dec.), 931–949.

Busso, M., Gallino, R., and Wasserburg, G. J. 1999. Nucleosynthesis in Asymptotic Giant Branch Stars: Relevance for Galactic Enrichment and Solar System Formation. *Annual Review of Astronomy and Astrophysics*, **37**(Jan.), 239–309.

Caffau, E., Bonifacio, P., François, P., Sbordone, L., Monaco, L., Spite, M., Spite, F., Ludwig, H.-G., Cayrel, R., Zaggia, S., Hammer, F., Randich, S., Molaro, P., and Hill, V. 2011. An extremely primitive star in the Galactic halo. *Nature*, **477**(Sept.), 67–69.

Carollo, D., Beers, T. C., Lee, Y. S., Chiba, M., Norris, J. E., Wilhelm, R., Sivarani, T., Marsteller, B., Munn, J. A., Bailer-Jones, C. A. L., Fiorentin, P. R., and York, D. G. 2007. Two stellar components in the halo of the Milky Way. *Nature*, **450**(Dec.), 1020–1025.

Carollo, D., Beers, T. C., Chiba, M., Norris, J. E., Freeman, K. C., Lee, Y. S., Ivezić, Ž., Rockosi, C. M., and Yanny, B. 2010. Structure and Kinematics of the Stellar Halos and Thick Disks of the Milky Way Based on Calibration Stars from Sloan Digital Sky Survey DR7. *ApJ*, **712**(Mar.), 692–727.

Casagrande, L., Schönrich, R., Asplund, M., Cassisi, S., Ramírez, I., Meléndez, J., Bensby, T., and Feltzing, S. 2011. New constraints on the chemical evolution of the solar neighbourhood and Galactic disc(s). Improved astrophysical parameters for the Geneva-Copenhagen Survey. *A&A*, **530**(June), A138.

Catelan, M. 2009. Horizontal branch stars: the interplay between observations and theory, and insights into the formation of the Galaxy. *Ap&SS*, **320**(Apr.), 261–309.

Chaplin, W. J., and Miglio, A. 2013. Asteroseismology of Solar-Type and Red-Giant Stars. *ARA&A*, **51**(Aug.), 353–392.

Chiappini, C., Matteucci, F., and Gratton, R. 1997. The Chemical Evolution of the Galaxy: The Two-Infall Model. *ApJ*, **477**(Mar.), 765–780.

Chiappini, C., Matteucci, F., and Ballero, S. K. 2005. The origin of nitrogen. Implications of recent measurements of N/O in Galactic metal-poor halo stars. *A&A*, **437**(July), 429–436.

Chiavassa, A., Plez, B., Josselin, E., and Freytag, B. 2009. Radiative hydrodynamics simulations of red supergiant stars. I. interpretation of interferometric observations. *A&A*, **506**(Nov.), 1351–1365.

Chiavassa, A., Pasquato, E., Jorissen, A., Sacuto, S., Babusiaux, C., Freytag, B., Ludwig, H.-G., Cruzalèbes, P., Rabbia, Y., Spang, A., and Chesneau, O. 2011. Radiative hydrodynamic simulations of red supergiant stars. III. Spectro-photocentric variability, photometric variability, and consequences on Gaia measurements. *A&A*, **528**(Apr.), A120.

Choplin, A., Hirschi, R., Meynet, G., and Ekström, S. 2017. Are some CEMP-s stars the daughters of spinstars? *A&A*, **607**(Nov.), L3.

Clarkson, O., Herwig, F., and Pignatari, M. 2018. Pop III i-process nucleosynthesis and the elemental abundances of SMSS J0313-6708 and the most iron-poor stars. *MNRAS*, **474**(Feb.), L37–L41.

Collet, R., Asplund, M., and Trampedach, R. 2007. Three-dimensional hydrodynamical simulations of surface convection in red giant stars. Impact on spectral line formation and abundance analysis. *A&A*, **469**(July), 687–706.

Curir, A., Lattanzi, M. G., Spagna, A., Matteucci, F., Murante, G., Re Fiorentin, P., and Spitoni, E. 2012. The thick disk rotation-metallicity correlation as a fossil of an "inverse chemical gradient" in the early Galaxy. *A&A*, **545**(Sept.), A133.

Danilovic, S., Solanki, S. K., Livingston, W., Krivova, N., and Vince, I. 2016. Variation of the Mn I 539.4 nm line with the solar cycle. *A&A*, **587**(Mar.), A33.

Dardelet, L., Ritter, C., Prado, P., Heringer, E., Higgs, C., Sandalski, S., Jones, S., Denisenkov, P., Venn, K., Bertolli, M., Pignatari, M., Woodward, P., and Herwig, F. 2014. i process and CEMP-s+r stars. Page 145 of: *XIII Nuclei in the Cosmos (NIC XIII)*.

Davies, B., Kudritzki, R.-P., Plez, B., Trager, S., Lançon, A., Gazak, Z., Bergemann, M., Evans, C., and Chiavassa, A. 2013. The Temperatures of Red Supergiants. *ApJ*, **767**(Apr.), 3.

Deason, A. J., Van der Marel, R. P., Guhathakurta, P., Sohn, S. T., and Brown, T. M. 2013. The Velocity Anisotropy of Distant Milky Way Halo Stars from Hubble Space Telescope Proper Motions. *ApJ*, **766**(Mar.).

Dravins, D. 1999. Stellar Surface Convection, Line Asymmetries, and Wavelength Shifts. Page 268 of: Hearnshaw, J. B., and Scarfe, C. D. (eds), *IAU Colloq. 170: Precise Stellar Radial Velocities*. Astronomical Society of the Pacific Conference Series, vol. 185.

Drout, M. R., Piro, A. L., Shappee, B. J., Kilpatrick, C. D., Simon, J. D., Contreras, C., Coulter, D. A., Foley, R. J., Siebert, M. R., Morrell, N., Boutsia, K., Di Mille, F., Holoien, T. W.-S., Kasen, D., Kollmeier, J. A., Madore, B. F., Monson, A. J., Murguia-Berthier, A., Pan, Y.-C., Prochaska, J. X., Ramirez-Ruiz, E., Rest, A., Adams, C., Alatalo, K., Bañados, E., Baughman, J., Beers, T. C., Bernstein, R. A., Bitsakis, T., Campillay, A., Hansen, T. T., Higgs, C. R., Ji, A. P., Maravelias, G., Marshall, J. L., Bidin, C. M., Prieto, J. L., Rasmussen, K. C., Rojas-Bravo, C., Strom, A. L., Ulloa, N., Vargas-González, J., Wan, Z., and Whitten, D. D. 2017. Light curves of the neutron star merger GW170817/SSS17a: Implications for r-process nucleosynthesis. *Science*, **358**(Dec.), 1570–1574.

El-Badry, K., Bland-Hawthorn, J., Wetzel, A., Quataert, E., Weisz, D. R., Boylan-Kolchin, M., Hopkins, P. F., Faucher-Giguère, C.-A., Kereš, D., and Garrison-Kimmel, S. 2018. Where are the most ancient stars in the Milky Way? *ArXiv e-prints*, Apr.

Evans, C. J., Davies, B., Kudritzki, R.-P., Puech, M., Yang, Y., Cuby, J.-G., Figer, D. F., Lehnert, M. D., Morris, S. L., and Rousset, G. 2011. Stellar metallicities beyond the Local Group: the potential of J-band spectroscopy with extremely large telescopes. *A&A*, **527**(Mar.), A50.

Ferraro, F. R., Sabbi, E., Gratton, R., Piotto, G., Lanzoni, B., Carretta, E., Rood, R. T., Sills, A., Fusi Pecci, F., Moehler, S., Beccari, G., Lucatello, S., and Compagni, N. 2006. Discovery of Carbon/Oxygen-depleted Blue Straggler Stars in 47 Tucanae: The Chemical Signature of a Mass Transfer Formation Process. *ApJ*, **647**(Aug.), L53–L56.

Fields, B. 2012 (Oct.). The Universe as an Accelerator: The Primordial Lithium Problem and Dark Matter. Page PB.001 of: *APS Division of Nuclear Physics Meeting Abstracts*.

Font, A. S., McCarthy, I. G., Crain, R. A., Theuns, T., Schaye, J., Wiersma, R. P. C., and Dalla Vecchia, C. 2011. Cosmological simulations of the formation of the stellar haloes around disc galaxies. *MNRAS*, **416**(Oct.), 2802–2820.

Frebel, A. 2010. Stellar archaeology: Exploring the Universe with metal-poor stars. *Astronomische Nachrichten*, **331**(May), 474–488.

Frebel, A., and Norris, J. E. 2015. Near-Field Cosmology with Extremely Metal-Poor Stars. *ARA&A*, **53**(Aug.), 631–688.

Freytag, B., and Höfner, S. 2008. Three-dimensional simulations of the atmosphere of an AGB star. *A&A*, **483**(May), 571–583.

Freytag, B., Holweger, H., Steffen, M., and Ludwig, H.-G. 1997. On the Scale of Photospheric Convection. Page 316 of: Paresce, F. (ed), *Science with the VLT Interferometer*.

Freytag, B., Steffen, M., and Dorch, B. 2002. Spots on the surface of Betelgeuse – Results from new 3D stellar convection models. *Astronomische Nachrichten*, **323**(July), 213–219.

Freytag, B., Steffen, M., Ludwig, H.-G., Wedemeyer-Böhm, S., Schaffenberger, W., and Steiner, O. 2012. Simulations of stellar convection with CO5BOLD. *Journal of Computational Physics*, **231**(Feb.), 919–959.

Freytag, B., Liljegren, S., and Höfner, S. 2017. Global 3D radiation-hydrodynamics models of AGB stars. Effects of convection and radial pulsations on atmospheric structures. *A&A*, **600**(Apr.), A137.

Frischknecht, U., Hirschi, R., Pignatari, M., Maeder, A., Meynet, G., Chiappini, C., Thielemann, F.-K., Rauscher, T., Georgy, C., and Ekström, S. 2016. s-process production in rotating massive stars at solar and low metallicities. *MNRAS*, **456**(Feb.), 1803–1825.

Fröhlich, C., Martínez-Pinedo, G., Liebendörfer, M., Thielemann, F.-K., Bravo, E., Hix, W. R., Langanke, K., and Zinner, N. T. 2006. Neutrino-Induced Nucleosynthesis of A64 Nuclei: The νp Process. *Physical Review Letters*, **96**(14), 142502.

Gaia Collaboration, Babusiaux, C., van Leeuwen, F., Barstow, M. A., Jordi, C., Vallenari, A., Bossini, D., Bressan, A., Cantat-Gaudin, T., van Leeuwen, M., Brown, A. G. A., Prusti, T., de Bruijne, J. H. J., Bailer-Jones, C. A. L., Biermann, M., Evans, D. W., Eyer, L., Jansen, F., Klioner, S. A., Lammers, U., Lindegren, L., Luri, X., Mignard, F., Panem, C., Pourbaix, D., Randich, S., Sartoretti, P., Siddiqui, H. I., Soubiran, C., Walton, N. A., Arenou, F., Bastian, U., Cropper, M., Drimmel, R., Katz, D., Lattanzi, M. G., Bakker, J., Cacciari, C., Castañeda, J., Chaoul, L., Cheek, N., DeAngeli, F., Fabricius, C., Guerra, R., Holl, B., Masana, E., Messineo, R., Mowlavi, N.,

Nienartowicz, K., Panuzzo, P., Portell, J., Riello, M., Seabroke, G. M., Tanga, P., Thévenin, F., Gracia-Abril, G., Comoretto, G., Garcia-Reinaldos, M., Teyssier, D., Altmann, M., Andrae, R., Audard, M., Bellas-Velidis, I., Benson, K., Berthier, J., Blomme, R., Burgess, P., Busso, G., Carry, B., Cellino, A., Clementini, G., Clotet, M., Creevey, O., Davidson, M., DeRidder, J., Delchambre, L., Dell'Oro, A., Ducourant, C., Fernández- Hernández, J., Fouesneau, M., Frémat, Y., Galluccio, L., García-Torres, M., González-Núñez, J., González-Vidal, J. J., Gosset, E., Guy, L. P., Halbwachs, J. L., Hambly, N. C., Harrison, D. L., Hernández, J., Hestroffer, D., Hodgkin, S. T., Hutton, A., Jasniewicz, G., Jean-Antoine-Piccolo, A., Jordan, S., Korn, A. J., Krone-Martins, A., Lanzafame, A. C., Lebzelter, T., Löffler, W., Manteiga, M., Marrese, P. M., Martín-Fleitas, J. M., Moitinho, A., Mora, A., Muinonen, K., Osinde, J., Pancino, E., Pauwels, T., Petit, J. M., Recio-Blanco, A., Richards, P. J., Rimoldini, L., Robin, A. C., Sarro, L. M., Siopis, C., Smith, M., Sozzetti, A., Süveges, M., Torra, J., vanReeven, W., Abbas, U., Abreu Aramburu, A., Accart, S., Aerts, C., Altavilla, G., Álvarez, M. A., Alvarez, R., Alves, J., Anderson, R. I., Andrei, A. H., Anglada Varela, E., Antiche, E., Antoja, T., Arcay, B., Astraatmadja, T. L., Bach, N., Baker, S. G., Balaguer-Núñez, L., Balm, P., Barache, C., Barata, C., Barbato, D., Barblan, F., Barklem, P. S., Barrado, D., Barros, M., Bartholomé Muñoz, S., Bassilana, J. L., Becciani, U., Bellazzini, M., Berihuete, A., Bertone, S., Bianchi, L., Bienaymé, O., Blanco-Cuaresma, S., Boch, T., Boeche, C., Bombrun, A., Borrachero, R., Bouquillon, S., Bourda, G., Bragaglia, A., Bramante, L., Breddels, M. A., Brouillet, N., Brüsemeister, T., Brugaletta, E., Bucciarelli, B., Burlacu, A., Busonero, D., Butkevich, A. G., Buzzi, R., Caffau, E., Cancelliere, R., Cannizzaro, G., Carballo, R., Carlucci, T., Carrasco, J. M., Casamiquela, L., Castellani, M., Castro-Ginard, A., Charlot, P., Chemin, L., Chiavassa, A., Cocozza, G., Costigan, G., Cowell, S., Crifo, F., Crosta, M., Crowley, C., Cuypers, J., Dafonte, C., Damerdji, Y., Dapergolas, A., David, P., David, M., deLaverny, P., DeLuise, F., DeMarch, R., deMartino, D., deSouza, R., deTorres, A., Debosscher, J., delPozo, E., Delbo, M., Delgado, A., Delgado, H. E., Diakite, S., Diener, C., Distefano, E., Dolding, C., Drazinos, P., Durán, J., Edvardsson, B., Enke, H., Eriksson, K., Esquej, P., Eynard Bontemps, G., Fabre, C., Fabrizio, M., Faigler, S., Falcão, A. J., Farràs Casas, M., Federici, L., Fedorets, G., Fernique, P., Figueras, F., Filippi, F., Findeisen, K., Fonti, A., Fraile, E., Fraser, M., Frézouls, B., Gai, M., Galleti, S., Garabato, D., García-Sedano, F., Garofalo, A., Garralda, N., Gavel, A., Gavras, P., Gerssen, J., Geyer, R., Giacobbe, P., Gilmore, G., Girona, S., Giuffrida, G., Glass, F., Gomes, M., Granvik, M., Gueguen, A., Guerrier, A., Guiraud, J., Gutiérrez-Sánchez, R., Haigron, R., Hatzidimitriou, D., Hauser, M., Haywood, M., Heiter, U., Helmi, A., Heu, J., Hilger, T., Hobbs, D., Hofmann, W., Holland, G., Huckle, H. E., Hypki, A., Icardi, V., Janßen, K., JevardatdeFombelle, G., Jonker, P. G., Juhász, Á. L., Julbe, F., Karampelas, A., Kewley, A., Klar, J., Kochoska, A., Kohley, R., Kolenberg, K., Kontizas, M., Kontizas, E., Koposov, S. E., Kordopatis, G., Kostrzewa-Rutkowska, Z., Koubsky, P., Lambert, S., Lanza, A. F., Lasne, Y., Lavigne, J. B., LeFustec, Y., LePoncin-Lafitte, C., Lebreton, Y., Leccia, S., Leclerc, N., Lecoeur-Taibi, I., Lenhardt, H., Leroux, F., Liao, S., Licata, E., Lindstrøm, H. E. P., Lister, T. A., Livanou, E., Lobel, A., López, M., Managau, S., Mann, R. G., Mantelet, G., Marchal, O., Marchant, J. M., Marconi, M., Marinoni, S., Marschalkó, G., Marshall, D. J., Martino, M., Marton, G., Mary, N., Massari, D., Matijevič, G., Mazeh, T., McMillan, P. J., Messina, S., Michalik, D., Millar, N. R., Molina, D., Molinaro, R., Molnár, L., Montegriffo, P., Mor, R., Morbidelli, R., Morel, T., Morris, D., Mulone, A. F., Muraveva, T., Musella, I., Nelemans, G., Nicastro, L., Noval, L., O'Mullane, W., Ordénovic, C., Ordóñez-Blanco, D., Osborne, P., Pagani, C., Pagano, I., Pailler,

F., Palacin, H., Palaversa, L., Panahi, A., Pawlak, M., Piersimoni, A. M., Pineau, F. X., Plachy, E., Plum, G., Poggio, E., Poujoulet, E., Prša, A., Pulone, L., Racero, E., Ragaini, S., Rambaux, N., Ramos-Lerate, M., Regibo, S., Reylé, C., Riclet, F., Ripepi, V., Riva, A., Rivard, A., Rixon, G., Roegiers, T., Roelens, M., Romero-Gómez, M., Rowell, N., Royer, F., Ruiz-Dern, L., Sadowski, G., Sagristà Sellés, T., Sahlmann, J., Salgado, J., Salguero, E., Sanna, N., Santana- Ros, T., Sarasso, M., Savietto, H., Schultheis, M., Sciacca, E., Segol, M., Segovia, J. C., Ségransan, D., Shih, I-C., Siltala, L., Silva, A. F., Smart, R. L., Smith, K. W., Solano, E., Solitro, F., Sordo, R., SoriaNieto, S., Souchay, J., Spagna, A., Spoto, F., Stampa, U., Steele, I. A., Steidelmüller, H., Stephenson, C. A., Stoev, H., Suess, F. F., Surdej, J., Szabados, L., Szegedi-Elek, E., Tapiador, D., Taris, F., Tauran, G., Taylor, M. B., Teixeira, R., Terrett, D., Teyssandier, P., Thuillot, W., Titarenko, A., TorraClotet, F., Turon, C., Ulla, A., Utrilla, E., Uzzi, S., Vaillant, M., Valentini, G., Valette, V., vanElteren, A., Van Hemelryck, E., Vaschetto, M., Vecchiato, A., Veljanoski, J., Viala, Y., Vicente, D., Vogt, S., vonEssen, C., Voss, H., Votruba, V., Voutsinas, S., Walmsley, G., Weiler, M., Wertz, O., Wevers, T., Wyrzykowski, Ł., Yoldas, A., Žerjal, M., Ziaeepour, H., Zorec, J., Zschocke, S., Zucker, S., Zurbach, C., and Zwitter, T. 2018. Gaia Data Release 2: Observational Hertzsprung-Russell diagrams. *ArXiv e-prints*, Apr.

Gautschy, A., and Saio, H. 1995. Stellar Pulsations Across The HR Diagram: Part 1. *ARA&A*, **33**, 75–114.

Gehren, T., Shi, J. R., Zhang, H. W., Zhao, G., and Korn, A. J. 2006. Na, Mg and Al abundances as a population discriminant for nearby metal-poor stars. *A&A*, **451**(June), 1065–1079.

Genovali, K., Lemasle, B., Bono, G., Romaniello, M., Fabrizio, M., Ferraro, I., Iannicola, G., Laney, C. D., Nonino, M., Bergemann, M., Buonanno, R., François, P., Inno, L., Kudritzki, R.-P., Matsunaga, N., Pedicelli, S., Primas, F., and Thévenin, F. 2014. On the fine structure of the Cepheid metallicity gradient in the Galactic thin disk. *A&A*, **566**(June), A37.

Gilmore, G., and Wyse, R. F. G. 1998. Element Ratios and the Formation of the Stellar Halo. *AJ*, **116**(Aug.), 748–753.

Goetz, M., and Koeppen, J. 1992. On abundance gradients in spiral galaxies. *A&A*, **262**(Sept.), 455–467.

Griffen, B. F., Dooley, G. A., Ji, A. P., O'Shea, B. W., Gómez, F. A., and Frebel, A. 2018. Tracing the first stars and galaxies of the Milky Way. *MNRAS*, **474**(Feb.), 443–459.

Gustafsson, B., Edvardsson, B., Eriksson, K., Jørgensen, U. G., Nordlund, Å., and Plez, B. 2008. A grid of MARCS model atmospheres for late-type stars. I. Methods and general properties. *A&A*, **486**(Aug.), 951–970.

Hall, J. C. 2008. Stellar Chromospheric Activity. *Living Reviews in Solar Physics*, **5**(Mar.), 2.

Hampel, M., Stancliffe, R. J., Lugaro, M., and Meyer, B. S. 2016. The Intermediate Neutron-capture Process and Carbon-enhanced Metal-poor Stars. *ApJ*, **831**(Nov.), 171.

Hansen, C. J., Nordström, B., Bonifacio, P., Spite, M., Andersen, J., Beers, T. C., Cayrel, R., Spite, F., Molaro, P., Barbuy, B., Depagne, E., François, P., Hill, V., Plez, B., and Sivarani, T. 2011. First stars. XIII. Two extremely metal-poor RR Lyrae stars. *A&A*, **527**(Mar.), A65.

Hansen, C. J., Primas, F., Hartman, H., Kratz, K.-L., Wanajo, S., Leibundgut, B., Farouqi, K., Hallmann, O., Christlieb, N., and Nilsson, H. 2012. Silver and palladium help unveil the nature of a second r-process. *A&A*, **545**(Sept.), A31.

Hansen, C. J., Montes, F., and Arcones, A. 2014. How Many Nucleosynthesis Processes Exist at Low Metallicity? *ApJ*, **797**(Dec.), 123.

Hansen, C. J., Nordström, B., Hansen, T. T., Kennedy, C. R., Placco, V. M., Beers, T. C., Andersen, J., Cescutti, G., and Chiappini, C. 2016a. Abundances of carbon-enhanced metal-poor stars as constraints on their formation. *A&A*, **588**(Apr.), A37.

Hansen, C. J., El-Souri, M., Monaco, L., Villanova, S., Bonifacio, P., Caffau, E., and Sbordone, L. 2018a. Ages and Heavy Element Abundances from Very Metal-poor Stars in the Sagittarius Dwarf Galaxy. *ApJ*, **855**(Mar.), 83.

Hansen, T. T., Andersen, J., Nordström, B., Beers, T. C., Placco, V. M., Yoon, J., and Buchhave, L. A. 2016b. The role of binaries in the enrichment of the early Galactic halo. III. Carbon-enhanced metal-poor stars - CEMP-s stars. *A&A*, **588**(Apr.), A3.

Hansen, T. T., Holmbeck, E. M., Beers, T. C., Placco, V. M., Roederer, I. U., Frebel, A., Sakari, C. M., Simon, J. D., and Thompson, I. B. 2018b. The *R*-Process Alliance: First Release from the Southern Search for *r*-Process-Enhanced Stars in the Galactic Halo. *ArXiv e-prints*, Apr.

Hauschildt, P. H., Allard, F., and Baron, E. 1999. The NextGen Model Atmosphere Grid for 3000=T_{eff}=10,000 K. *ApJ*, **512**(Feb.), 377–385.

Hawkins, K., Masseron, T., Jofré, P., Gilmore, G., Elsworth, Y., and Hekker, S. 2016. An accurate and self-consistent chemical abundance catalogue for the APOGEE/Kepler sample. *A&A*, **594**(Oct.), A43.

Heger, A., and Woosley, S. E. 2002. The Nucleosynthetic Signature of Population III. *ApJ*, **567**(Mar.), 532–543.

Hill, V., Christlieb, N., Beers, T. C., Barklem, P. S., Kratz, K.-L., Nordström, B., Pfeiffer, B., and Farouqi, K. 2017. The Hamburg/ESO R-process Enhanced Star survey (HERES). XI. The highly r-process-enhanced star CS 29497-004. *A&A*, **607**(Nov.), A91.

Holmberg, J., Nordström, B., and Andersen, J. 2009. The Geneva-Copenhagen survey of the solar neighbourhood. III. Improved distances, ages, and kinematics. *A&A*, **501**(July), 941–947.

Honda, S., Aoki, W., Ishimaru, Y., and Wanajo, S. 2007. Neutron-Capture Elements in the Very Metal-poor Star HD 88609: Another Star with Excesses of Light Neutron-Capture Elements. *ApJ*, **666**(Sept.), 1189–1197.

Ito, H., Aoki, W., Beers, T. C., Tominaga, N., Honda, S., and Carollo, D. 2013. Chemical Analysis of the Ninth Magnitude Carbon-enhanced Metal-poor Star BD+44deg 493. *ApJ*, **773**(*Aug.*), 33.

José, J., and Iliadis, C. 2011. Nuclear astrophysics: the unfinished quest for the origin of the elements. *Reports on Progress in Physics*, **74**(9), 096901.

Karakas, A. I., and Lattanzio, J. C. 2014. The Dawes Review 2: Nucleosynthesis and Stellar Yields of Low- and Intermediate-Mass Single Stars. , **31**(July), e030.

Karlsson, T. 2005. Stochastic chemical enrichment in metal-poor systems. I. Theory. *A&A*, **439**(Aug.), 93–106.

Karlsson, T., and Gustafsson, B. 2005. Stochastic chemical enrichment in metal-poor systems. II. Abundance ratios and scatter. *A&A*, **436**(June), 879–894.

Kasen, D., Metzger, B., Barnes, J., Quataert, E., and Ramirez-Ruiz, E. 2017. Origin of the heavy elements in binary neutron-star mergers from a gravitational-wave event. *Nature*, **551**(Nov.), 80–84.

Keller, S. C., Bessell, M. S., Frebel, A., Casey, A. R., Asplund, M., Jacobson, H. R., Lind, K., Norris, J. E., Yong, D., Heger, A., Magic, Z., da Costa, G. S., Schmidt, B. P., and Tisserand, P. 2014. A single low-energy, iron-poor supernova as the source of metals in the star SMSS J031300.36-670839.3. *Nature*, **506**(Feb.), 463–466.

Kirby, E. N., Cohen, J. G., Smith, G. H., Majewski, S. R., Sohn, S. T., and Guhathakurta, P. 2011. Multi-element Abundance Measurements from Medium-resolution Spectra. IV. Alpha Element Distributions in Milky Way Satellite Galaxies. *ApJ*, **727**(Feb.), 79.

Kurucz, R. L. 1993 (Jan.). A New Opacity-Sampling Model Atmosphere Program for Arbitrary Abundances. Page 87 of: Dworetsky, M. M., Castelli, F., and Faraggiana, R. (eds), *IAU Colloq. 138: Peculiar versus Normal Phenomena in A-type and Related Stars*. Astronomical Society of the Pacific Conference Series, vol. 44.

Lacey, C. G., and Fall, S. M. 1983. Kinematical and chemical evolution of the galactic disc. *MNRAS*, **204**(Aug.), 791–810.

Laporte, C. F. P., Johnston, K. V., Gómez, F. A., Garavito-Camargo, N., and Besla, G. 2017. The Influence of Sagittarius and the Large Magellanic Cloud on the Milky Way Galaxy. *ArXiv e-prints*, Oct.

Lattanzio, J., Frost, C., Cannon, R., and Wood, P. R. 1996. Hot bottom burning in intermediate mass stars. *Mem. Soc. Astron. Italiana*, **67**, 729.

Leaman, R. 2012. Insights into Pre-enrichment of Star Clusters and Self-enrichment of Dwarf Galaxies from Their Intrinsic Metallicity Dispersions. *AJ*, **144**(Dec.), 183.

Lee, Y. S., Beers, T. C., An, D., Ivezić, Ž., Just, A., Rockosi, C. M., Morrison, H. L., Johnson, J. A., Schönrich, R., Bird, J., Yanny, B., Harding, P., and Rocha-Pinto, H. J. 2011. Formation and Evolution of the Disk System of the Milky Way: [α/Fe] Ratios and Kinematics of the SEGUE G-dwarf Sample. *ApJ*, **738**(Sept.), 187.

Lee, Y. S., Beers, T. C., Masseron, T., Plez, B., Rockosi, C. M., Sobeck, J., Yanny, B., Lucatello, S., Sivarani, T., Placco, V. M., and Carollo, D. 2013. Carbon-enhanced Metal-poor Stars in SDSS/SEGUE. I. Carbon Abundance Estimation and Frequency of CEMP Stars. *AJ*, **146**(Nov.), 132.

Lee, Y.-W. 1992. Evidence for an old Galactic bulge from RR Lyrae stars in Baade's window - Implications for the formation of the Galaxy and the age of the universe. *AJ*, **104**(Nov.), 1780–1789.

Leenaarts, J., Carlsson, M., and Rouppe van der Voort, L. 2012. The Formation of the Hα Line in the Solar Chromosphere. *ApJ*, **749**(Apr.), 136.

Lind, K., Amarsi, A. M., Asplund, M., Barklem, P. S., Bautista, M., Bergemann, M., Collet, R., Kiselman, D., Leenaarts, J., and Pereira, T. M. D. 2017. Non-LTE line formation of Fe in late-type stars - IV. Modelling of the solar centre-to-limb variation in 3D. *MNRAS*, **468**(July), 4311–4322.

Linsky, J. L. 2017. Stellar Model Chromospheres and Spectroscopic Diagnostics. *ARA&A*, **55**(Aug.), 159–211.

Ludwig, H.-G. 2006. Hydrodynamical simulations of convection-related stellar microvariability. I. Statistical relations for photometric and photocentric variability. *A&A*, **445**(Jan.), 661–671.

Madore, B. F., and Freedman, W. L. 1998. Calibration of the Extragalactic Distance Scale. Page 263 of: Aparicio, A., Herrero, A., and Sánchez, F. (eds), *Stellar astrophysics for the local group: VIII Canary Islands Winter School of Astrophysics*.

Maeder, A. 1990. Tables for massive star evolution at various metallicities. *Astronomy and Astrophysics Supplement Series*, **84**(July), 139–177.

Mannucci, F., Della Valle, M., and Panagia, N. 2006. Two populations of progenitors for Type Ia supernovae? *MNRAS*, **370**(Aug.), 773–783.

Marconi, M., and Minniti, D. 2018. Gauging the Helium Abundance of the Galactic Bulge RR Lyrae Stars. *ApJ*, **853**(Feb.), L20.

Martig, M., Fouesneau, M., Rix, H.-W., Ness, M., Mészáros, S., García-Hernández, D. A., Pinsonneault, M., Serenelli, A., Silva Aguirre, V., and Zamora, O. 2016. Red giant

masses and ages derived from carbon and nitrogen abundances. *MNRAS*, **456**(Mar.), 3655–3670.

Martin, D., Perego, A., Arcones, A., Thielemann, F.-K., Korobkin, O., and Rosswog, S. 2015. Neutrino-driven Winds in the Aftermath of a Neutron Star Merger: Nucleosynthesis and Electromagnetic Transients. *ApJ*, **813**(Nov.), 2.

Mashonkina, L., Christlieb, N., and Eriksson, K. 2014. The Hamburg/ESO R-process Enhanced Star survey (HERES). X. HE 2252-4225, one more r-process enhanced and actinide-boost halo star. *A&A*, **569**(Sept.), A43.

Matteucci, F., and Calura, F. 2005. Early chemical enrichment of the universe and the role of very massive population III stars. *MNRAS*, **360**(June), 447–452.

Matteucci, F., and Greggio, L. 1986. Relative roles of type I and II supernovae in the chemical enrichment of the interstellar gas. *A&A*, **154**(Jan.), 279–287.

McCarthy, I. G., Font, A. S., Crain, R. A., Deason, A. J., Schaye, J., and Theuns, T. 2012. Global structure and kinematics of stellar haloes in cosmological hydrodynamic simulations. *MNRAS*, **420**(Mar.), 2245–2262.

Merrill, P. W. 1952. Spectroscopic Observations of Stars of Class. *ApJ*, **116**(July), 21.

Metzger, B. D., Martínez-Pinedo, G., Darbha, S., Quataert, E., Arcones, A., Kasen, D., Thomas, R., Nugent, P., Panov, I. V., and Zinner, N. T. 2010. Electromagnetic counterparts of compact object mergers powered by the radioactive decay of r-process nuclei. *MNRAS*, **406**(Aug.), 2650–2662.

Mikolaitis, Š., Hill, V., Recio-Blanco, A., de Laverny, P., Allende Prieto, C., Kordopatis, G., Tautvaišiene, G., Romano, D., Gilmore, G., Randich, S., Feltzing, S., Micela, G., Vallenari, A., Alfaro, E. J., Bensby, T., Bragaglia, A., Flaccomio, E., Lanzafame, A. C., Pancino, E., Smiljanic, R., Bergemann, M., Carraro, G., Costado, M. T., Damiani, F., Hourihane, A., Jofré, P., Lardo, C., Magrini, L., Maiorca, E., Morbidelli, L., Sbordone, L., Sousa, S. G., Worley, C. C., and Zaggia, S. 2014. The Gaia-ESO Survey: the chemical structure of the Galactic discs from the first internal data release. *A&A*, **572**(Dec.), A33.

Mösta, P., Roberts, L. F., Halevi, G., Ott, C. D., Lippuner, J., Haas, R., and Schnetter, E. 2017. R-process Nucleosynthesis from Three-Dimensional Magnetorotational Core-Collapse Supernovae. *ArXiv e-prints*, Dec.

Nardetto, N., Gieren, W., Kervella, P., Fouqué, P., Storm, J., Pietrzynski, G., Mourard, D., and Queloz, D. 2009. High-resolution spectroscopy for Cepheids distance determination. V. Impact of the cross-correlation method on the p-factor and the γ-velocities. *A&A*, **502**(Aug.), 951–956.

Ness, M., Hogg, D. W., Rix, H.-W., Martig, M., Pinsonneault, M. H., and Ho, A. Y. Q. 2016. Spectroscopic Determination of Masses (and Implied Ages) for Red Giants. *ApJ*, **823**(June), 114.

Neyskens, P., van Eck, S., Jorissen, A., Goriely, S., Siess, L., and Plez, B. 2015. The temperature and chronology of heavy-element synthesis in low-mass stars. *Nature*, **517**(Jan.), 174–176.

Nishimura, N., Sawai, H., Takiwaki, T., Yamada, S., and Thielemann, F.-K. 2017. The Intermediate r-process in Core-collapse Supernovae Driven by the Magneto-rotational Instability. *ApJ*, **836**(Feb.), L21.

Nissen, P. E., and Schuster, W. J. 1997. Chemical composition of halo and disk stars with overlapping metallicities. *A&A*, **326**(Oct.), 751–762.

Nissen, P. E., and Schuster, W. J. 2010. Two distinct halo populations in the solar neighborhood. Evidence from stellar abundance ratios and kinematics. *A&A*, **511**(Feb.), L10.

Nordlander, T., Amarsi, A. M., Lind, K., Asplund, M., Barklem, P. S., Casey, A. R., Collet, R., and Leenaarts, J. 2017. 3D NLTE analysis of the most iron-deficient star, SMSS0313-6708. *A&A*, **597**(Jan.), A6.

Nordlund, Å., Stein, R. F., and Asplund, M. 2009. Solar Surface Convection. *Living Reviews in Solar Physics*, **6**(Apr.), 2.

Osorio, Y., and Barklem, P. S. 2016. Mg line formation in late-type stellar atmospheres. II. Calculations in a grid of 1D models. *A&A*, **586**(Feb.), A120.

Parenago, P. P. 1945. Some work on the structure of the galaxy. *Popular Astronomy*, **53**(Dec.), 441.

Pian, E., D'Avanzo, P., Benetti, S., Branchesi, M., Brocato, E., Campana, S., Cappellaro, E., Covino, S., D'Elia, V., Fynbo, J. P. U., Getman, F., Ghirlanda, G., Ghisellini, G., Grado, A., Greco, G., Hjorth, J., Kouveliotou, C., Levan, A., Limatola, L., Malesani, D., Mazzali, P. A., Melandri, A., Møller, P., Nicastro, L., Palazzi, E., Piranomonte, S., Rossi, A., Salafia, O. S., Selsing, J., Stratta, G., Tanaka, M., Tanvir, N. R., Tomasella, L., Watson, D., Yang, S., Amati, L., Antonelli, L. A., Ascenzi, S., Bernardini, M. G., Boër, M., Bufano, F., Bulgarelli, A., Capaccioli, M., Casella, P., Castro-Tirado, A. J., Chassande-Mottin, E., Ciolfi, R., Copperwheat, C. M., Dadina, M., De Cesare, G., di Paola, A., Fan, Y. Z., Gendre, B., Giuffrida, G., Giunta, A., Hunt, L. K., Israel, G. L., Jin, Z.-P., Kasliwal, M. M., Klose, S., Lisi, M., Longo, F., Maiorano, E., Mapelli, M., Masetti, N., Nava, L., Patricelli, B., Perley, D., Pescalli, A., Piran, T., Possenti, A., Pulone, L., Razzano, M., Salvaterra, R., Schipani, P., Spera, M., Stamerra, A., Stella, L., Tagliaferri, G., Testa, V., Troja, E., Turatto, M., Vergani, S. D., and Vergani, D. 2017. Spectroscopic identification of r-process nucleosynthesis in a double neutron-star merger. *Nature*, **551**(Nov.), 67–70.

Placco, V. M., Frebel, A., Beers, T. C., and Stancliffe, R. J. 2014. Carbon-enhanced Metal-poor Star Frequencies in the Galaxy: Corrections for the Effect of Evolutionary Status on Carbon Abundances. *ApJ*, **797**(Dec.), 21.

Placco, V. M., Holmbeck, E. M., Frebel, A., Beers, T. C., Surman, R. A., Ji, A. P., Ezzeddine, R., Points, S. D., Kaleida, C. C., Hansen, T. T., Sakari, C. M., and Casey, A. R. 2017. RAVE J203843.2-002333: The First Highly R-process-enhanced Star Identified in the RAVE Survey. *ApJ*, **844**(July), 18.

Pont, F., Mayor, M., and Burki, G. 1994. New radial velocities for classical cepheids. Local galactic rotation revisited. *A&A*, **285**(May), 415–439.

Ramírez, I., Allende Prieto, C., and Lambert, D. L. 2008. Granulation in K-type dwarf stars. I. Spectroscopic observations. *A&A*, **492**(Dec.), 841–855.

Riess, A. G., Macri, L., Casertano, S., Lampeitl, H., Ferguson, H. C., Filippenko, A. V., Jha, S. W., Li, W., and Chornock, R. 2011. A 3% Solution: Determination of the Hubble Constant with the Hubble Space Telescope and Wide Field Camera 3. *ApJ*, **730**(Apr.), 119.

Ruchti, G. R., Bergemann, M., Serenelli, A., Casagrande, L., and Lind, K. 2013. Unveiling systematic biases in the 1D LTE excitation-ionization balance of Fe for FGK stars: a novel approach to determination of stellar parameters. *MNRAS*, **429**(Feb.), 126–134.

Rybizki, J., Just, A., and Rix, H.-W. 2017. Chempy: A flexible chemical evolution model for abundance fitting. Do the Sun's abundances alone constrain chemical evolution models? *A&A*, **605**(Sept.), A59.

Salaris, M. 2012. Distance indicators from colour-magnitude-diagrams: main sequence, red clump and tip of the RGB. *Ap&SS*, **341**(Sept.), 65–75.

Sbordone, L., Bonifacio, P., Caffau, E., Ludwig, H.-G., Behara, N. T., González Hernández, J. I., Steffen, M., Cayrel, R., Freytag, B., van't Veer, C., Molaro, P., Plez, B., Sivarani, T., Spite, M., Spite, F., Beers, T. C., Christlieb, N., François, P., and Hill, V. 2010. The

metal-poor end of the Spite plateau. I. Stellar parameters, metallicities, and lithium abundances. *A&A*, **522**(Nov.), A26.

Schönrich, R., and McMillan, P. J. 2017. Understanding inverse metallicity gradients in galactic discs as a consequence of inside-out formation. *MNRAS*, **467**(May), 1154–1174.

Schönrich, Ralph, and Binney, James. 2009a. Chemical evolution with radial mixing. *MNRAS*, **396**(June), 203–222.

Schönrich, Ralph, and Binney, James. 2009b. Origin and structure of the Galactic disc(s). *MNRAS*, **399**(Nov.), 1145–1156.

Schönrich, Ralph, Asplund, Martin, and Casagrande, Luca. 2011. On the alleged duality of the Galactic halo. *MNRAS*, **415**(Aug.), 3807–3823.

Schönrich, Ralph, Asplund, Martin, and Casagrande, Luca. 2014. Does SEGUE/SDSS indicate a dual Galactic halo? *ApJ*, **786**(May).

Schwarzschild, M. 1975. On the scale of photospheric convection in red giants and supergiants. *ApJ*, **195**(Jan.), 137–144.

Searle, L., and Zinn, R. 1978. Composition of halo clusters and the formation of the galactic halo. *ApJ*, **225**(Oct.), 357–379.

Seitenzahl, I. R., and Townsley, D. M. 2017. Nucleosynthesis in thermonuclear supernovae. *ArXiv e-prints*, Apr.

Seitenzahl, I. R., Cescutti, G., Röpke, F. K., Ruiter, A. J., and Pakmor, R. 2013. Solar abundance of manganese: a case for near Chandrasekhar-mass Type Ia supernova progenitors. *A&A*, **559**(Nov.), L5.

Sellwood, J. A., and Binney, J. J. 2002. Radial mixing in galactic discs. *MNRAS*, **336**(Nov.), 785–796.

Serenelli, A., Weiss, A., Cassisi, S., Salaris, M., and Pietrinferni, A. 2017. The brightness of the red giant branch tip. Theoretical framework, a set of reference models, and predicted observables. *A&A*, **606**(Oct.), A33.

Shappee, B. J., Simon, J. D., Drout, M. R., Piro, A. L., Morrell, N., Prieto, J. L., Kasen, D., Holoien, T. W.-S., Kollmeier, J. A., Kelson, D. D., Coulter, D. A., Foley, R. J., Kilpatrick, C. D., Siebert, M. R., Madore, B. F., Murguia-Berthier, A., Pan, Y.-C., Prochaska, J. X., Ramirez-Ruiz, E., Rest, A., Adams, C., Alatalo, K., Bañados, E., Baughman, J., Bernstein, R. A., Bitsakis, T., Boutsia, K., Bravo, J. R., Di Mille, F., Higgs, C. R., Ji, A. P., Maravelias, G., Marshall, J. L., Placco, V. M., Prieto, G., and Wan, Z. 2017. Early spectra of the gravitational wave source GW170817: Evolution of a neutron star merger. *Science*, **358**(Dec.), 1574–1578.

Siqueira Mello, C., Spite, M., Barbuy, B., Spite, F., Caffau, E., Hill, V., Wanajo, S., Primas, F., Plez, B., Cayrel, R., Andersen, J., Nordström, B., Sneden, C., Beers, T. C., Bonifacio, P., François, P., and Molaro, P. 2013. First stars. XVI. HST/STIS abundances of heavy elements in the uranium-rich metal-poor star CS 31082-001. *A&A*, **550**(Feb.), A122.

Smartt, S. J., Chen, T.-W., Jerkstrand, A., Coughlin, M., Kankare, E., Sim, S. A., Fraser, M., Inserra, C., Maguire, K., Chambers, K. C., Huber, M. E., Krühler, T., Leloudas, G., Magee, M., Shingles, L. J., Smith, K. W., Young, D. R., Tonry, J., Kotak, R., Gal-Yam, A., Lyman, J. D., Homan, D. S., Agliozzo, C., Anderson, J. P., Angus, C. R., Ashall, C., Barbarino, C., Bauer, F. E., Berton, M., Botticella, M. T., Bulla, M., Bulger, J., Cannizzaro, G., Cano, Z., Cartier, R., Cikota, A., Clark, P., De Cia, A., Della Valle, M., Denneau, L., Dennefeld, M., Dessart, L., Dimitriadis, G., Elias-Rosa, N., Firth, R. E., Flewelling, H., Flörs, A., Franckowiak, A., Frohmaier, C., Galbany, L., González-Gaitán, S., Greiner, J., Gromadzki, M., Guelbenzu, A. N., Gutiérrez, C. P., Hamanowicz, A., Hanlon, L., Harmanen, J., Heintz, K. E., Heinze,

A., Hernandez, M.-S., Hodgkin, S. T., Hook, I. M., Izzo, L., James, P. A., Jonker, P. G., Kerzendorf, W. E., Klose, S., Kostrzewa-Rutkowska, Z., Kowalski, M., Kromer, M., Kuncarayakti, H., Lawrence, A., Lowe, T. B., Magnier, E. A., Manulis, I., Martin-Carrillo, A., Mattila, S., McBrien, O., Müller, A., Nordin, J., O'Neill, D., Onori, F., Palmerio, J. T., Pastorello, A., Patat, F., Pignata, G., Podsiadlowski, P., Pumo, M. L., Prentice, S. J., Rau, A., Razza, A., Rest, A., Reynolds, T., Roy, R., Ruiter, A. J., Rybicki, K. A., Salmon, L., Schady, P., Schultz, A. S. B., Schweyer, T., Seitenzahl, I. R., Smith, M., Sollerman, J., Stalder, B., Stubbs, C. W., Sullivan, M., Szegedi, H., Taddia, F., Taubenberger, S., Terreran, G., van Soelen, B., Vos, J., Wainscoat, R. J., Walton, N. A., Waters, C., Weiland, H., Willman, M., Wiseman, P., Wright, D. E., Wyrzykowski, Ł., and Yaron, O. 2017. A kilonova as the electromagnetic counterpart to a gravitational-wave source. *Nature*, **551**(Nov.), 75–79.

Sneden, C., Cowan, J. J., Lawler, J. E., Ivans, I. I., Burles, S., Beers, T. C., Primas, F., Hill, V., Truran, J. W., Fuller, G. M., Pfeiffer, B., and Kratz, K.-L. 2003. The Extremely Metal-poor, Neutron Capture-rich Star CS 22892-052: A Comprehensive Abundance Analysis. *ApJ*, **591**(July), 936–953.

Soderblom, D. R. 2010. The Ages of Stars. *ARA&A*, **48**(Sept.), 581–629.

Soszyński, I., Udalski, A., Szymański, M. K., Pietrukowicz, P., Mróz, P., Skowron, J., Kozłowski, S., Poleski, R., Skowron, D., Pietrzyński, G., Wyrzykowski, L., Ulaczyk, K., and Kubiak, M. 2014. Over 38000 RR Lyrae Stars in the OGLE Galactic Bulge Fields. , **64**(Sept.), 177–196.

Spagna, A., Lattanzi, M. G., Re Fiorentin, P., and Smart, R. L. 2010. Evidence of a thick disk rotation-metallicity correlation. *A&A*, **510**(Feb.), L4.

Spina, L., Meléndez, J., Karakas, A. I., Ramírez, I., Monroe, T. R., Asplund, M., and Yong, D. 2016. Nucleosynthetic history of elements in the Galactic disk. [X/Fe]-age relations from high-precision spectroscopy. *A&A*, **593**(Oct.), A125.

Spite, M., Cayrel, R., Plez, B., Hill, V., Spite, F., Depagne, E., François, P., Bonifacio, P., Barbuy, B., Beers, T., Andersen, J., Molaro, P., Nordström, B., and Primas, F. 2005. First stars VI - Abundances of C, N, O, Li, and mixing in extremely metal-poor giants. Galactic evolution of the light elements. *A&A*, **430**(Feb.), 655–668.

Spite, M., Caffau, E., Bonifacio, P., Spite, F., Ludwig, H.-G., Plez, B., and Christlieb, N. 2013. Carbon-enhanced metal-poor stars: the most pristine objects? *A&A*, **552**(Apr.), A107.

Spite, M., Peterson, R. C., Gallagher, A. J., Barbuy, B., and Spite, F. 2017. Abundances of the light elements from UV (HST) and red (ESO) spectra in the very old star HD 84937. *A&A*, **600**(Apr.), A26.

Starkenburg, E., Hill, V., Tolstoy, E., François, P., Irwin, M. J., Boschman, L., Venn, K. A., de Boer, T. J. L., Lemasle, B., Jablonka, P., Battaglia, G., Groot, P., and Kaper, L. 2013. The extremely low-metallicity tail of the Sculptor dwarf spheroidal galaxy. *A&A*, **549**(Jan.), A88.

Starkenburg, E., Oman, K. A., Navarro, J. F., Crain, R. A., Fattahi, A., Frenk, C. S., Sawala, T., and Schaye, J. 2017. The oldest and most metal-poor stars in the APOSTLE Local Group simulations. *MNRAS*, **465**(Feb.), 2212–2224.

Steigman, G. 2007. Primordial Nucleosynthesis in the Precision Cosmology Era. *Annual Review of Nuclear and Particle Science*, **57**(Nov.), 463–491.

Stibbs, D. W. N. 1956. On the differential galactic rotation of the system of cepheid variable stars. *MNRAS*, **116**, 453.

Tajitsu, A., Sadakane, K., Naito, H., Arai, A., and Aoki, W. 2015. Explosive lithium production in the classical nova V339 Del (Nova Delphini 2013). *Nature*, **518**(Feb.), 381–384.

Tanvir, N. R., Levan, A. J., Fruchter, A. S., Hjorth, J., Hounsell, R. A., Wiersema, K., and Tunnicliffe, R. L. 2013. A 'kilonova' associated with the short-duration γ-ray burst GRB 130603B. *Nature*, **500**(Aug.), 547–549.

Thielemann, F.-K., Fröhlich, C., Hirschi, R., Liebendörfer, M., Dillmann, I., Mocelj, D., Rauscher, T., Martinez-Pinedo, G., Langanke, K., Farouqi, K., Kratz, K.-L., Pfeiffer, B., Panov, I., Nadyozhin, D. K., Blinnikov, S., Bravo, E., Hix, W. R., Höflich, P., and Zinner, N. T. 2007. Production of intermediate-mass and heavy nuclei. *Progress in Particle and Nuclear Physics*, **59**(July), 74–93.

Thielemann, F.-K., Eichler, M., Panov, I. V., and Wehmeyer, B. 2017. Neutron Star Mergers and Nucleosynthesis of Heavy Elements. *Annual Review of Nuclear and Particle Science*, **67**(Oct.), 253–274.

Thompson, B. B., Few, C. G., Bergemann, M., Gibson, B. K., MacFarlane, B. A., Serenelli, A., Gilmore, G., Randich, S., Vallenari, A., Alfaro, E. J., Bensby, T., Francois, P., Korn, A. J., Bayo, A., Carraro, G., Casey, A. R., Costado, M. T., Donati, P., Franciosini, E., Frasca, A., Hourihane, A., Jofré, P., Hill, V., Heiter, U., Koposov, S. E., Lanzafame, A., Lardo, C., de Laverny, P., Lewis, J., Magrini, L., Marconi, G., Masseron, T., Monaco, L., Morbidelli, L., Pancino, E., Prisinzano, L., Recio-Blanco, A., Sacco, G., Sousa, S. G., TautvaišienÄ–, G., Worley, C. C., and Zaggia, S. 2018. The Gaia-ESO Survey: matching chemodynamical simulations to observations of the Milky Way. *MNRAS*, **473**(Jan.), 185–197.

Tinsley, B. M. 1979. Stellar lifetimes and abundance ratios in chemical evolution. *ApJ*, **229**(May), 1046–1056.

Tissera, P. B., Scannapieco, C., Beers, T. C., and Carollo, D. 2013. Stellar haloes of simulated Milky-Way-like galaxies: chemical and kinematic properties. *MNRAS*, **432**(July), 3391–3400.

Tissera, P. B., Beers, T. C., Carollo, D., and Scannapieco, C. 2014. Stellar haloes in Milky Way mass galaxies: from the inner to the outer haloes. *MNRAS*, **439**(Apr.), 3128–3138.

Tissera, P. B., Machado, R. E. G., Carollo, D., Minniti, D., Beers, T. C., Zoccali, M., and Meza, A. 2018. The central spheroids of Milky Way mass-sized galaxies. *MNRAS*, **473**(Jan.), 1656–1666.

Tolstoy, E., Hill, V., and Tosi, M. 2009. Star-Formation Histories, Abundances, and Kinematics of Dwarf Galaxies in the Local Group. *ARA&A*, **47**(Sept.), 371–425.

Trampedach, R., Asplund, M., Collet, R., Nordlund, Å., and Stein, R. F. 2013. A Grid of Three-dimensional Stellar Atmosphere Models of Solar Metallicity. I. General Properties, Granulation, and Atmospheric Expansion. *ApJ*, **769**(May), 18.

Travaglio, C., Rauscher, T., Heger, A., Pignatari, M., and West, C. 2018. Role of Core-collapse Supernovae in Explaining Solar System Abundances of p Nuclides. *ApJ*, **854**(Feb.), 18.

Tremblay, P.-E., Ludwig, H.-G., Freytag, B., Steffen, M., and Caffau, E. 2013. Granulation properties of giants, dwarfs, and white dwarfs from the CIFIST 3D model atmosphere grid. *A&A*, **557**(Sept.), A7.

Vasilyev, V., Ludwig, H.-G., Freytag, B., Lemasle, B., and Marconi, M. 2017. Spectroscopic properties of a two-dimensional time-dependent Cepheid model. I. Description and validation of the model. *A&A*, **606**(Oct.), A140.

Viallet, M., and Baraffe, I. 2012. Scenarios to explain extreme Be depletion in solar-like stars: accretion or rotation effects? *A&A*, **546**(Oct.), A113.

Wallerstein, G. 2002. The Cepheids of Population II and Related Stars. *PASP*, **114**(July), 689–699.

Wanajo, S., Janka, H.-T., and Müller, B. 2011. Electron-capture Supernovae as The Origin of Elements Beyond Iron. *ApJ*, **726**(Jan.), L15.

White, S. D. M., and Springel, V. 2000. Where Are the First Stars Now? Page 327 of: Weiss, A., Abel, T. G., and Hill, V. (eds), *The First Stars*.

White, Simon D. M., and Frenk, Carlos S. 1991. Galaxy Formation through Hierarchical Clustering. *ApJ*, **379**(Sept.), 52.

Wielen, R. 1974. Space Velocities of Nearby Classical Cepheids. *A&AS*, **15**(Apr.).

Yoon, J., Beers, T. C., Placco, V. M., Rasmussen, K. C., Carollo, D., He, S., Hansen, T. T., Roederer, I. U., and Zeanah, J. 2016. Observational Constraints on First-star Nucleosynthesis. I. Evidence for Multiple Progenitors of CEMP-No Stars. *ApJ*, **833**(Dec.), 20.

Zhang, B. R., Childress, M. J., Davis, T. M., Karpenka, N. V., Lidman, C., Schmidt, B. P., and Smith, M. 2017. A blinded determination of H_0 from low-redshift Type Ia supernovae, calibrated by Cepheid variables. *MNRAS*, **471**(Oct.), 2254–2285.

Author index

Subject index